ACS OMEGA

Open Access
This article is licensed under CC-BY-NC-ND 4.0

http://pubs.acs.org/journal/acsodf
Article

Comprehensive Investigation of the Adsorption, Corrosion Inhibitory Properties, and Quantum Calculations for 2-(2,4,5-Trimethoxybenzylidene) Hydrazine Carbothioamide in Mitigating Corrosion of XC38 Carbon Steel under HCl Environment

Nadia Mouats, Souad Djellali, Hana Ferkous,* Amel Sedik, Amel Delimi, Abir Boublia, Khadidja Otmane Rachedi, Malika Berredjem, Alaaddin Çukurovali, Manawwer Alam, Barbara Ernsti, and Yacine Benguerba*

Cite This: *ACS Omega* 2024, 9, 27945−27962

Read Online
ACCESS | Metrics & More | Article Recommendations

ABSTRACT: This study investigates the inhibitory effects of 2-(2,4,5-trimethoxy benzylidene) hydrazine carbothioamide (TMBHCA) on the corrosion of carbon steel in a 1 M HCl solution across various concentrations. The assessment employs a comprehensive approach, combining gravimetric analysis, potentiodynamic polarization tests, and electrochemical impedance spectroscopy (EIS). Additionally, scanning electron microscopy (SEM) and quantum chemical calculations are employed to provide a thorough understanding of the corrosion inhibition mechanism. The influence of exposure time on mild steel corrosion is systematically examined. Results reveal a remarkable reduction in the corrosion rate of steel, with TMBHCA demonstrating its highest inhibition efficiency of 97.8% at 200 ppm. Potentiodynamic polarization studies characterize TMBHCA as a mixed-type inhibitor, while Nyquist plots illustrate increased charge transfer resistance and decreased double-layer capacitance with escalating TMBHCA concentrations. Consistency between weight loss measurements and electrochemical findings further validates the efficacy of TMBHCA as a corrosion inhibitor. SEM images substantiate and visually support the obtained results. An immersion test conducted at 25 °C over 28 days showcases a notable enhancement in TMBHCA efficiency (IE%) from 45.16% to 92.43% at 200 ppm as the immersion period progresses from 1 day to 28 days. This improvement is attributed to the augmented adsorption of inhibitor molecules on the steel surface over time. These comprehensive findings significantly contribute to our understanding of TMBHCA's corrosion inhibition behavior, emphasizing its potential as a highly efficient corrosion inhibitor for diverse industrial applications.

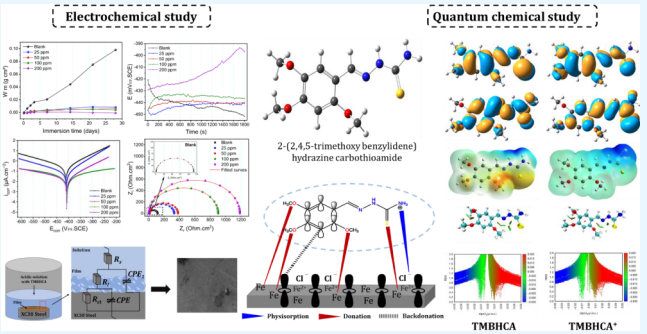

1. INTRODUCTION

Carbon steel finds widespread application in high-tech industries owing to its commendable mechanical and physical properties.[1] However, its use in aggressive environments leads to corrosion, posing a significant challenge across various industries.[2] The economic implications of its usage are profound, given that steel-based infrastructures are the backbone of modern economies. Despite its strengths, carbon steel's susceptibility to corrosion when exposed to aggressive environments poses a formidable challenge, incurring substantial financial losses across various sectors. Corrosion's impact on the economy is not to be underestimated, as it is estimated that effective corrosion prevention techniques could slash prevention and maintenance costs by 15% to 35%, which translates to significant savings in the context of large-scale industrial operations.[3]

Health considerations are increasingly paramount in the selection of corrosion prevention methods. Traditional inhibitors often contain toxic substances that pose risks to human health and the environment.[4−6] In response to these concerns, the industry's focus has shifted toward developing corrosion inhibitors that are nontoxic, economically viable, and environmentally friendly. Schiff bases have emerged as a

Received: December 21, 2023
Revised: June 2, 2024
Accepted: June 6, 2024
Published: June 15, 2024

© 2024 The Authors. Published by American Chemical Society

https://doi.org/10.1021/acsomega.3c10240
ACS Omega 2024, 9, 27945−27962

promising class of organic inhibitors, offering effective corrosion resistance without the associated health risks.[7−10]

Production processes in industries such as petrochemical, maritime, and construction, where carbon steel is predominantly used, have been forced to reevaluate their corrosion mitigation strategies due to stricter environmental regulations and the demand for more sustainable practices. The deterioration of steel in these sectors not only requires costly maintenance but also leads to operational inefficiencies and, in worst-case scenarios, catastrophic failures that can have severe environmental and health repercussions.[11,12]

Recent literature further substantiates the urgency for more efficient and safer corrosion inhibitors. Studies have indicated that the shift toward green corrosion inhibitors is not only a matter of environmental and health concern but also of economic benefit. Innovative inhibitors that minimize toxic waste and resource expenditure are being highlighted as keys to sustainable industrial growth.[13,14] Organic inhibitors, particularly those functioning through adsorption, have been the subject of extensive research, with studies delving into their mechanisms of action through electrostatic and charge-sharing interactions.[15−18]

The efficiency of these inhibitors is closely linked to their molecular structures. The presence of appropriate functional groups, aromaticity, and the electron density of donor atoms contribute significantly to their adsorption properties and, by extension, their inhibition performance.[19−22] In addition, quantum chemical techniques have become indispensable in disentangling the complexities of these molecular interactions, providing a deeper understanding that aids in the design of more effective inhibitors.[23,24]

In contrast to several potent organic inhibitors that incorporate toxic and costly elements, contemporary endeavors are concentrated on the creation of corrosion inhibitors that are nontoxic, economically viable, and environmentally friendly, with Schiff bases being a notable example. Schiff bases, with a broad functional range, have applications in catalysis, corrosion inhibition, analytical chemistry, medicine, and photochromics.[25−28] Their efficacy as corrosion inhibitors for diverse metals and alloys, particularly in challenging environments, has been firmly established.[29,30] Schiff bases display notable corrosion inhibition characteristics, featuring a C−N group, an electron cloud present on the aromatic ring, and heteroatoms such as nitrogen, oxygen, and sulfur with electronegative properties.[13,31−33] Their popularity stems from their cost-effectiveness, ease of synthesis, and minimal environmental footprint, which align with current industry trends toward more sustainable materials.[34,35]

This investigation centers on examining the inhibitory effects of 2-(2,4,5-trimethoxybenzylidene) hydrazine carbothioamide (TMBHCA) on carbon steel XC38 immersed in a 1 M HCl solution. The assessment encompasses gravimetric (weight loss) analyses, potentiodynamic polarization, and electrochemical impedance spectroscopy (EIS) techniques, coupled with scanning electron microscopy (SEM) for visual examination. Thermodynamic and kinetic parameters are computed to ascertain the inhibition mechanism. Additionally, the study delves into adsorption parameters and employs density functional theory (DFT) calculations to elucidate the molecular behavior and electron interactions occurring at the metal interface. This research introduces a novel perspective by unraveling the corrosion inhibition properties of TMBHCA and elucidating its intricate molecular interactions with carbon steel in aggressive acidic environments.

2. MATERIALS AND METHODS

2.1. Structural Analysis, Sample Preparation, and Solution Formulation. The inhibitor under examination is a Schiff base known as 2-(2,4,5-trimethoxy benzylidene) hydrazine carbothioamide (TMBHCA), and its structural representation is illustrated in Figure 1.

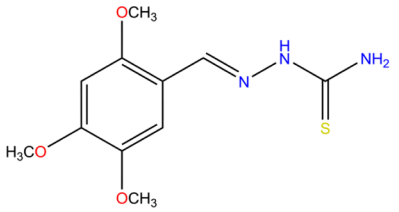

Figure 1. Molecular structure of TMBHCA; molar mass = 269.319 g·mol^{-1}, formula = $C_{11}H_{15}N_3O_3S$.

In this investigation, the material of interest is carbon steel XC38, characterized by the specified nominal elemental composition of the material that includes carbon (C: 0.38%), silicon (Si: 0.27%), manganese (Mn: 0.66%), nickel (Ni: 0.02%), chromium (Cr: 0.21%), and molybdenum (Mo: 0.02%), with the remaining balance consisting of iron (Fe). Samples extracted from this metal are employed in both the gravimetric analysis and SEM examinations. These specimens are fashioned into rod shapes with 2 × 0.5 × 0.2 cm^3 dimensions. However, for the electrochemical assessments, cylindrical specimens are utilized and fixed in an inert resin. Before each utilization, the exposed surface area (0.27 cm^2) is meticulously polished via sandpaper of diverse grits, cleansed with double-distilled water, and degreased with aceton.

The corrosive medium is prepared by diluting a reagent-grade 37% weight HCl aqueous solution with distilled water to achieve a 1 M hydrochloric acid (HCl) solution. Notably, TMBHCA solutions of different concentrations (ranging from 25 to 200 ppm) are formulated by dissolving the inhibitor in a 1 M hydrochloric acid solution (HCl), aided by 10% dimethyl sulfoxide (DMSO) as an organic solvent. This ensures proper solubility of the inhibitor in the corrosive medium, meeting one of the key criteria for evaluating its effectiveness as a corrosion inhibitor.

2.2. Gravimetric Analysis. Gravimetric measurements are performed by assessing weight loss in a 1 M HCl solution with varying concentrations of the TMBHCA inhibitor. Prior to immersion, samples undergo a series of preparations, including polishing, cleaning, degreasing, and drying. Subsequently, the treated samples are vertically immersed in the corrosive medium. Weights are recorded both before immersion and at various durations, ranging from 24 h (1 day) to 672 h (28 days). The corrosion rate (W_{corr}) is determined under different conditions using eq 1.

$$W_{corr} = \frac{\Delta_m}{S \cdot t} = \frac{m_1 - m_2}{S \cdot t} \quad (1)$$

Here, the symbols m_1 and m_2 signify the masses of the carbon steel sample prior to and following immersion in each corrosive solution, respectively, while S (cm^2) represents the sample surface area. The parameter t denotes the exposure time in hours in the studied medium. The inhibition

https://doi.org/10.1021/acsomega.3c10240
ACS Omega 2024, 9, 27945−27962

effectiveness, expressed as IE (%), is computed using the following expression:

$$\text{IE}\ (\%) = \frac{C_R - C_{R(i)}}{\text{CR}} \cdot 100 \tag{2}$$

2.3. Electrochemical Measurements. In the electrochemical analyses, a three-electrode electrochemical cell is employed, with carbon steel serving as the working electrode (WE), platinum serving as the counter electrode (CE), and a saturated Ag/AgCl electrode acting as the reference electrode (RE). The open circuit potential (OCP) is determined initially to assess the stability of the corrosion potential of the freshly polished metal immersed in the corrosive environment (1 M HCl) for 30 min until a stable state is achieved. Subsequently, potentiodynamic polarization (PDP) curves are acquired by scanning the potential range from −0.20 V/Ag/AgCl to +0.20 V/Ag/AgCl, with respect to the OCP, employing a scanning rate of 1 $mV{\cdot}s^{-1}$. The inhibition efficiency (E_{icorr}%) is determined from the Tafel plot using the subsequent equation:

$$E_{\text{icorr}}\ (\%) = \frac{(i^0_{\text{corr}} - i_{\text{corr}})}{i^0_{\text{corr}}} \cdot 100 \tag{3}$$

Here, i^0_{corr}, and i_{corr} represent the current densities in both uninhibited and inhibited solutions, respectively. The polarization resistance (R_p) in $ohm{\cdot}cm^2$ is determined using the Stern−Geary correlation as expressed in eq 4.

$$R_p = \frac{\beta_a \beta_c}{2.30 i_{\text{corr}}(\beta_a + \beta_c)} \tag{4}$$

where β_a and β_c are the anodic and cathodic Tafel slopes, respectively. E_{R_p} is given by

$$E_{R_p}\ (\%) = \frac{(R_p - R_p^0)}{R_p} \cdot 100 \tag{5}$$

R_p^0 and R_p are the polarization resistance values obtained before and after the addition of the inhibitor, respectively.

The EIS experiments were realized at an OCP, varying the frequency from 50 kHz to 10 mHz and a signal amplitude of 10 mV. The resulting data were utilized to estimate the inhibition effectiveness (E_{EIS}) using the following expression:

$$E_{\text{EIS}}\ (\%) = \frac{(R_{ct} - R_{ct}^0)}{R_{ct}} \cdot 100 \tag{6}$$

The surface coverage degree was also evaluated using

$$\theta = \frac{(R_{ct} - R_{ct}^0)}{R_{ct}} \tag{7}$$

where R_{ct} and R_{ct}^0 are the charge transfer resistances in the HCl medium in the presence and absence of the inhibitor, respectively.

2.4. Surface Analysis. The XC38 carbon steel specimens were immersed in a 1 M HCl solution for 24 h at room temperature, both with and without TMCBHA molecule at the optimal concentration (200 ppm). Before immersion, the specimens were individually prepared, cleaned, and dried with bidistilled water. The surface morphologies of both uninhibited and inhibited carbon steel samples were examined using a Tescan Vega 3 microscope operating at a 20-kV accelerating voltage.

2.5. DFT Theory Implantation. Throughout this investigation, quantum Chemica camputations were conducted via the Gaussian 09 W program package,[36,37] while the results were analyzed and visualized through GaussView 5.0.8 software.[38] Molecular structure optimization was performed employing DFT with Becke's three-parameter hybrid exchange functional and Lee−Yang−Parr correlation functionals (B3LYP).[39] The DFT calculations utilized the 6-31G (*d*,*p*) basis set.[40,41] Electronic characteristics of the most stable conformers were assessed to determine quantum chemical properties. The TMBHCA inhibitor was subjected to DFT-based quantum chemical computations in both neutral and protonated forms.[42] To establish correlations between molecular structures and anticorrosion activity, a variety of global and local molecular reactivity indices were calculated. Additionally, a non-covalent interaction (NCI) approach was employed as a robust method for investigating and visualizing weak interactions in three-dimensional space.[43,44] This analysis involved the computation of reduced density gradients (RDGs) and electron densities (ρ) according to the equation:

$$s = \frac{1}{2(3\pi^2)^{1/3}} \frac{|\nabla\rho|}{\rho^{4/3}} \tag{8}$$

Here, ρ signifies the electron density, and $\nabla\rho$ denotes its first derivative. NCI, encompassing interactions like hydrogen bonding (HB), van der Waals (vdw) interactions, and steric repulsions, was investigated at specific distances due to their potential impact on molecular behavior.[45,46] In this study, the NCI based on RDG was conducted using the Multiwfn program to observe the weak interactions within the system.[47] The NCI analysis based on RDG was conducted using the Multiwfn program, and the weak interactions within the system were observed and visualized using the visual molecular dynamics (VMD) interface.[48] Additionally, the components were graphically represented by gnuplot to generate color scatter graphs.[49]

3. RESULTS AND DISCUSSIONS

3.1. Impact of Inhibitor Concentrations. *3.1.1. Gravimetric Measurements.* The gravimetric method is a fundamental and widely utilized technique for assessing the mass loss of a metal due to corrosion after exposure to acidic environments. In this study, we explored the impact of introducing an inhibitor at concentrations ranging from 25 to 200 ppm on the corrosion of carbon steel in a 1 M HCl solution, employing weight-loss measurements at 298 K, as illustrated in Figure 2.

The inhibition efficiency (E_w %) was calculated using the formula:

$$E_w\ (\%) = \frac{W_{\text{corr}} - W'_{\text{corr}}}{W_{\text{corr}}} \times 100 \tag{9}$$

Here, W'_{corr} and W_{corr} represent the corrosion rates of the metal in HCl solutions with and without the inhibitor, respectively.

Table 1 presents the corrosion parameters, including corrosion rate (W_{corr}) and corrosion inhibition efficiency (E_w %), obtained through weight loss measurements for XC38 carbon steel specimens immersed in a 1 M HCl solution. The investigation explores the influence of various concentrations (50−200 ppm) of the TMBHCA inhibitor at an ambient temperature of 298 K. The results show a noticeable decrease

https://doi.org/10.1021/acsomega.3c10240
ACS Omega 2024, 9, 27945−27962

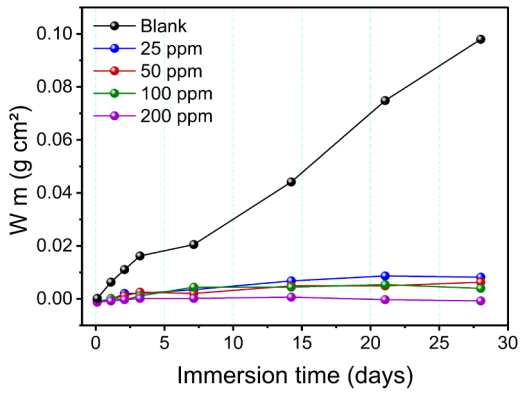

Figure 2. XC38 steel weight loss in 1 M HCl solutions at different TMBHCA concentrations with respect to immersion time (at T = 298 K).

Table 1. Corrosion Rate and Inhibition Effectiveness of Carbon Steel at Various Time Intervals in 1 M HCl Solution at Different TMBHCA Concentrations (298 K)

concentration (ppm)	Δ_m (g) × 10^{-3}	W_{corr} (g·cm^{-2}·h^{-1})^9 × 10^{-6}	E_w (%)
blank	44.3	15.9	-
25 ppm	7.2	2.47	84.46
50 ppm	5.7	1.87	88.23
100 ppm	5.4	1.59	90.00
200 ppm	0.9	0.3	**98.10**

in Δ_m as the concentration of the TMBHCA inhibitor increases, leading to a corresponding rise in inhibition efficiency, reaching 98.1% at 200 ppm. This phenomenon suggests the deposition of TMBHCA molecules on the XC38 carbon steel surface in the aggressive solution (1 M HCl), indicating effective protection. These outcomes suggest that the inhibitor serves as a robust protector.[50]

3.1.2. Open Circuit Potential (OCP) Measurements. The OCP curves play a crucial role in assessing the corrosion inhibition effectiveness of TMBHCA on XC38 steel. Figure 3 illustrates the OCP curves of XC38 in an HCl medium under various concentrations at 298 K, both in the absence and presence of the TMBHCA inhibitor.

As demonstrated in Figure 3, the OCP curve serves as a window into the thermodynamic equilibrium of the metal's surface in a corrosive milieu. The E_{ocp} acts as an indicator,

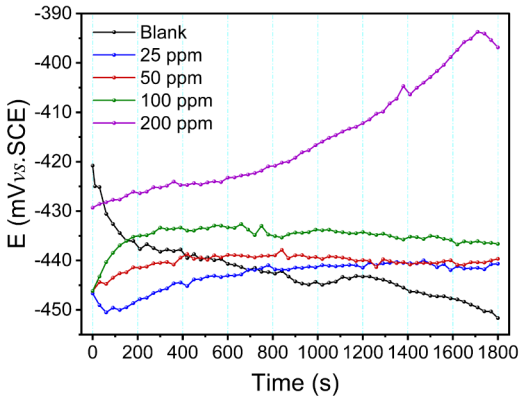

Figure 3. XC38 steel open circuit potential with and without TMCBHA inhibitor at different concentrations.

signaling the dynamic parity between the oxidative and reductive processes at the interval of the metal and the solution. The shifts in E_{ocp} with varying inhibitor concentrations provide a quantitative measure of TMBHCA's ability to fortify the steel against corrosion-induced degradation. The E_{ocp} value of the uncoated carbon steel electrode measured after 30 min in 1 M HCl solution was −0.450 V. In both situations, it is seen that the OCP rises over time before stabilizing after a predetermined amount of time. This is because the acid is constantly attacking the metal. But, when the inhibitor is not present, the OCP potential seems to start at a lower value than when the inhibitor is present, suggesting that the inhibitor has a major impact on the metal's dissolution. Furthermore, this suggests that the TMBHCA inhibitor may have an impact on both anodic and cathodic polarizations.[51,52]

3.1.3. Polarization Examination. Figure 4 shows the polarization curves attained following the submersion of

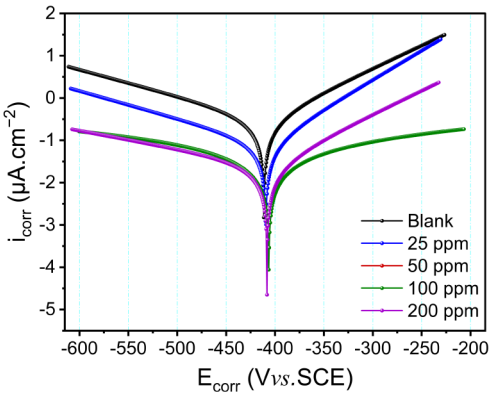

Figure 4. Potentiodynamic polarization curves of XC38 in a 1.0 M HCl solution in the absence and presence of TMBHCA at different concentrations.

XC38 carbon steel in acidic solutions (1 M HCl), in the presence and the absence of TMBHCA. Preliminary scrutiny of these curves reveals that the introduction of TMBHCA exerts a negligible effect on both the anodic and cathodic segments.[53−55] The extrapolation of Tafel polarization lines allows for the determination of various electrochemical parameters, including corrosion potential (E_{corr}), corrosion current density (i_{corr}), anodic Tafel slope (β_a), cathodic Tafel slope (β_c), and polarization resistance (R_p). The inhibition effectiveness is computed using eq 14 from Tafel plots, and the resulting parameters are succinctly presented in Table 2.

$$E_{icorr}\ (\%) = \frac{(i^0_{corr} - i_{corr})}{i^0_{corr}} \cdot 100 \tag{10}$$

Here, i_{corr} and i'_{corr} are the corrosion current densities of XC38 carbon steel in the blank (1 M HCl) and in the presence of an inhibitor, respectively.

Figure 4 provides a clear visual representation of the shift of both anodic and cathodic curves toward lower current densities upon the addition of the inhibitor, signifying the deceleration of carbon steel anodic dissolution. This observation implies that the inhibitor effectively retards both the anodic reaction of metal dissolution and the cathodic hydrogen evolution.

https://doi.org/10.1021/acsomega.3c10240
ACS Omega 2024, 9, 27945−27962

Table 2. Polarization Parameters of XC38 Carbon Steel Corrosion in 1 M HCl with Varying Concentrations of TMBCHA

parameters	E_{corr} (mV) (Ag/AgCl)	i_{corr} (μA·cm^{-2})	R_p (Ω·cm^2)	βa (mV/dec)	βc (mV/dec)	E_i (%)	E_{R_p} (%)
blank	−411.42	305.30	80.7	91.9	159.50	-	-
25 ppm	−409.31	142.82	246.0	72.2	152.3	53.23	67.19
50 ppm	−408.12	81.77	1081.0	89.2	231.9	73.21	92.53
100 ppm	−406.32	25.12	1202.0	73.3	866.9	91.77	93.28
200 ppm	−408.12	23.72	1296	89.2	231.9	92.23	**93.77**

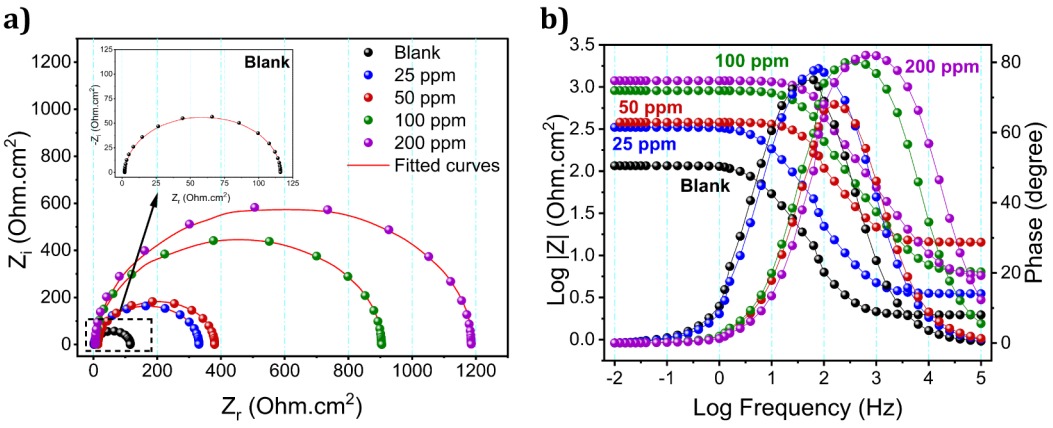

Figure 5. Nyquist (a) and (b) Bode plots of mild steel in 1 M HCl solution in the absence and presence of TMBHCA at different concentrations after 1 h of immersion.

Table 3. Electrochemical Impedance Spectroscopy Characteristics for the Carbon Steel Corrosion in 1 M HCl at Different TMCBAH Concentrations

		CPE			CPE$_1$						
C (ppm)	R_s (Ω·cm^2)	(F·s^1(a^{-1}))	n	R_1 (Ω·cm^2)	(F·s^1(a^{-1}))	n'	R_{ct} (Ω·cm^2)	x^2	x^2/|Z|	$X/N^{1/2}$	EI (%)
blank	2.334	2.61×10^{-04}	0.9904	113.8	-	-	-	603.9	0.635	3.838	
25 ppm	3.844	7.47×10^{-05}	0.9759	197.5	2.27×10^{-03}	0.017	188.3	3564	0.304	9.323	39.57
50 ppm	13.09	1.21×10^{-05}	0.9512	12.02	3.93×10^{-06}	1.000	359.6	2185	0.138	7.390	68.35
100 ppm	9.196	4.95×10^{-06}	0.9961	292.2	1.91×10^{-06}	1.000	606.3	12000	1.606	17.110	81.23
200 ppm	9.223	2.27×10^{-06}	0.9909	330	1.20×10^{-06}	0.990	854.6	24023	2.190	25.830	**86.68**

Electrochemical reactions at the metal's surface lead to metal dissolution, with the anodic and cathodic sites playing crucial roles. Inhibitors modulate the charge transfer mechanism at these sites to hinder metallic dissolution. In this instance, the functional groups present in TMBHCA comprise heteroatoms that facilitate the adsorption of inhibitor molecules onto the steel surface, establishing robust coordination interactions with the mild steel surface. Adsorption may take place through physisorption, chemisorption, or a combination of both. The reduction in the corrosion rate signifies the successful adsorption of inhibitor molecules on the metal surface, providing protection against corrosion.[56,57]

Table 2 illustrates that even a minimal quantity of the inhibitor markedly diminishes icorr. The i_{corr} of the blank solution decreases from 305.3 to 23.72 μA·cm^{-2} for 200 ppm of TMBHCA. Additionally, there is a noticeable increase in polarization resistance (R_p), rising from 80.7 to 1296 Ω·cm^2 without and with the inhibitor at 200 ppm, respectively. Table 2 also shows that the addition of the inhibitor does not cause a significant shift in the E_{corr} value. This indicates that the synthesized inhibitor acts as a mixed-type inhibitor, affecting both anodic and cathodic reactions.[58] These findings suggest that inhibitor molecules engage with the metal surface, obstructing active sites and enhancing protection against corrosion. Regarding efficiency values, it is evident that the inhibition efficiency of TMBHCA improves with increasing inhibitor concentration, reaching up to 93.77% at a concentration of 200 ppm. This improvement results from the enhancement of TMBHCA molecules on the XC38 surface, effectively protecting it in the acidic solution.

3.1.4. Electrochemical Impedance Spectroscopy (EIS). Electrochemical impedance spectroscopy (EIS) stands as a well-established and potent technique for corrosion mechanism, providing insights into surface properties.[59,60] The related Nyquist and Bode plots of MS obtained in 1 M HCl solution in the absence and presence of the inhibitor are shown in Figure 5a,b, respectively. Hence, the EIS data were fitted to experimental data, and the results are displayed in Table 3. For this purpose, two electrical equivalent circuit diagrams were suggested to define the XC38/solution interface. Where CPE stands for a constant phase element composed of Y_o and n. Solution resistance is denoted by R_s, while phase shift, or departure from an ideal capacitor and degree of surface inhomogeneity, is represented by n. Due to its superior representation of an actual system, a CPE element was chosen above a double-layer capacitance (C_{dl}).

As can be observed from Figure 5a, the Nyquist plots of the XC38 electrode obtained in the absence and presence of the TMBCHA show depressed semicircular forms. As the concentration of the inhibitor increases, so do the plot sizes.

https://doi.org/10.1021/acsomega.3c10240
ACS Omega 2024, 9, 27945−27962

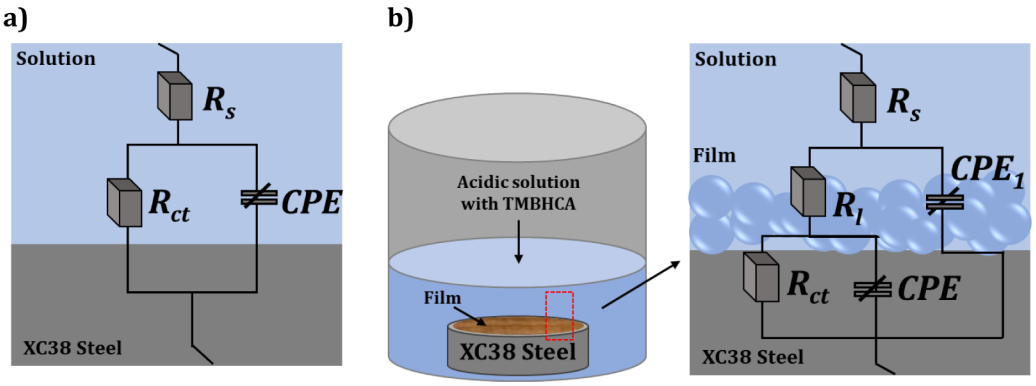

Figure 6. Proposed electrical equivalent circuit model for fitting impedance data points and its significance on the corrosion of XC38 steel without (a) and with the TMBHCA inhibitor (b).

It appears that the corrosion of XC38 in 1 M HCl solution primarily occurs *via* a charge transfer process because only one time constant showed up in the Nyguist plots. In the absence and presence of inhibitor at different concentrations, the diagram consists of a semicircle loop, which may be related to unstable adsorption intermediate molecules such $(FeCl)_{ads}$ and $(FeCl^{-}\ Inh^{+})_{ads}$.[61] The parallel observations could be detected from the corresponding Bode plots (Figure 5b). The similar observation has been reported in the literature for steel corrosion in HCl medium.

The capacitive semicircle is related to the charge transfer resistance (R_{ct}), diffuse layer resistance (R_d), and accumulation resistance at the mild steel/solution interface (R_a), which also provides a barrier effect. The total resistance is called the polarization resistance, R_p ($R_p = R_{ct} + R_d + R_a$).[62] In the inhibited solutions, the corrosion process is again activation-controlled. When the concentration reaches 200 ppm, the diameter of the depressed semicircle increases as it is related to R_p. In this case, the polarization resistance takes film resistance into account in addition to the previously discussed blank solution's. The observation that resistance and protection efficiency increase as TMBCHA concentration increases implies that a greater number of inhibitor molecules are able to adsorb on the metal surface, leading to a thicker surface film or higher surface coverage.[63−65]

As it is shown in Table 3, the *n* value being less than 1 is due to the metal/solution interface not behaving as an ideal capacitor. The reduction in double-layer capacitance (CPE) values in the presence of the TMBCHA inhibitor (from 2.61×10^{-04} $\mu F \cdot cm^{-2}$ to 2.27×10^{-06} $\mu F \cdot cm^{-2}$) is associated with the Helmholtz model, suggesting a substitution of H_2O molecules on the steel surface by inhibitor molecules. This decline signifies TMBCHA adsorption on the XC38 metal surface, creating a protecting layer with a reduction in the dissolution reaction degree. The correlation between these findings and data from weight loss and polarization experiments suggests a potential link to a reduced local dielectric constant and an increased electrical double-layer thickness.[65] Consequently, this inhibitor demonstrates effective protection for the metal. The inhibition efficiency (IE %), calculated using eq 15 is 90.33% at 200 ppm, indicating a significant limitation of XC38 carbon steel corrosion by HCl owing to the addition of TMBHCA.

$$\text{IE}\ (\%) = \frac{R'_{ct} - R_{ct}}{R'_{ct}} \cdot 100 \tag{11}$$

where R_{ct} and R'_{ct} signify the charge transfer resistances with and without the inhibitor, respectively.

Figure 6 depicts the equivalent circuit (EC) employed for analyzing impedance spectra. In this circuit, the constant phase element (CPE) is utilized to replace the double-layer capacitance, a choice made due to the presence of depressed capacitive loops observed in Nyquist plots. The inclusion of the CPE in the EC is a well-recognized approach in corrosion studies. This is because the macroscopic carefully weighed impedance is intricately linked to numerous microscopic material characteristics, including surface defects, local charge inhomogeneities, and numerous complicated electrochemical reactions.[66,67] The elements within the circuit include the R_s, CPE, R_l, and R_{ct}.

The inhibitor's introduction into the acidic solution improves the transfer resistance while concurrently minimizing the double-layer capacitance in the inhibitor's presence. The constant phase element undergoes a reduction akin to the observed corrosion current densities (i_{corr}) in this study. This decrease is ascribed to the adsorption of these compounds on the metal surface, resulting in the creation of an acidic solution film.

3.2. Impact of Immersion Time. The efficacy of TMBCHA as a corrosion inhibitor for mild steel in 1 M HCl was evaluated through meticulous EIS analysis over an extended immersion period of 28 days, conducted at a constant temperature of 25 °C. This investigation aimed to discern the long-term stability of TMBCHA's adsorption properties under conditions mimicking acid-cleaning operations. EIS analysis, illustrated in Figures 7 and 8 demonstrates a significant enhancement in corrosion inhibition performance correlated with increased immersion time. This trend indicates an optimal inhibition efficiency of 92.43% achieved at a concentration of 200 ppm after 28 days. The progressive increase in inhibition efficiency with time is attributed to the improved adsorption of TMBCHA molecules onto the surface of mild steel, thereby facilitating a denser and more protective barrier against corrosion in an aqueous HCl environment.[68−70]

The consistent trend observed in the EIS analysis, as depicted in Figures 7 and 8, further substantiates the impact of immersion time on the corrosion inhibition effectiveness of TMBCHA. As detailed in Figure 7, the Nyquist plots for XC38 carbon steel in 1 M HCl, both with and without 200 ppm of TMBCHA inhibitor, exhibit clear variations with changing immersion durations. As the immersion time progresses from 1 to 28 days, the Nyquist plots indicate a continuous

https://doi.org/10.1021/acsomega.3c10240
ACS Omega 2024, 9, 27945−27962

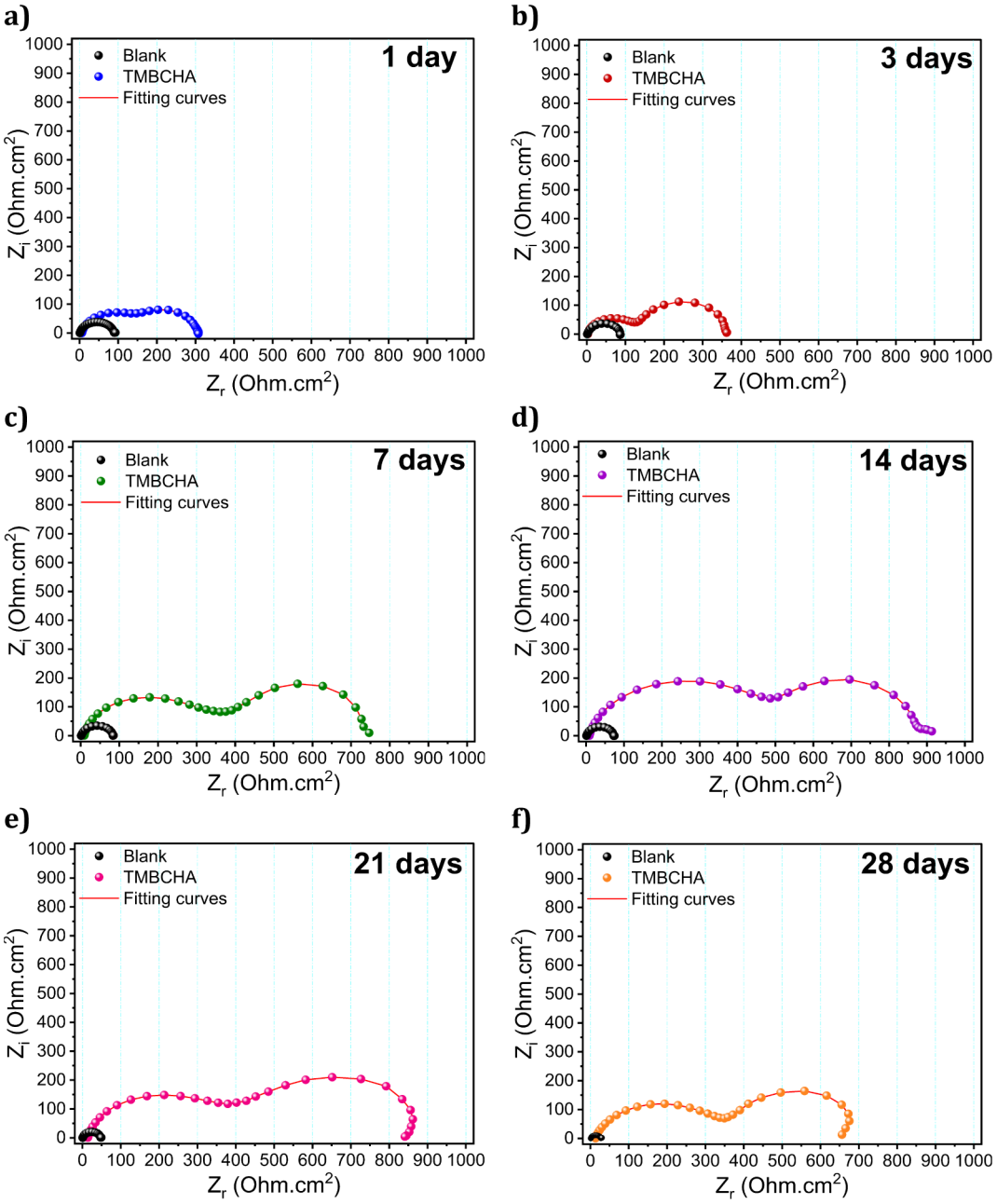

Figure 7. Immersion time effect on the Nyquist plots for XC38 carbon steel in 1 M HCl without and with 200 ppm of TMBCHA and at various immersion durations: (a) 1 day, (b) 3 days, (c) 7 days, (d) 14 days, (e) 21 days, and (f) 28 days.

improvement in the inhibition effectiveness of TMBCHA. This is reflected in the evolving impedance spectra, highlighting the inhibitor's enhanced ability to resist the corrosive effects on the carbon steel surface. As well, in Figure 8a, the Nyquist plots offer a detailed insight into the corrosion behavior of mild steel under different immersion durations for the blank solution. Figure 8b further supplements this information by presenting the Bode plot for the blank at various immersion times, revealing the presence of a second time constant in the system. Moving to Figure 8c,d, the Nyquist and Bode plots, respectively, provide a comprehensive perspective on mild steel's corrosion response under varying immersion durations in the presence of TMBCHA inhibitor. The noticeable alterations in the size and shape of the impedance spectra clearly underscore the influence of immersion time, emphasizing its significant impact on the corrosion inhibition effectiveness of TMBCHA.

Furthermore, the analysis of the EIS data, as presented in Table 4, provides valuable insights into the corrosion inhibition effectiveness of TMBCHA over varying immersion durations. The evolution of key parameters such as R_s, R_{ct}, and CPE offers a comprehensive understanding of the inhibitor's performance. For the blank sample, R_s decreases steadily from 1.063 Ω·cm^2 at 1 day to 0.996 Ω·cm^2 at 21 days before increasing slightly to 1.042 Ω·cm^2 at 28 days. In contrast, for TMBCHA-treated samples, R_s exhibits a different trend, starting at 5.988 Ω·cm^2 at 1 day, decreasing significantly to 2.563 Ω·cm^2 at 3 days, and then gradually increasing to 13.730 Ω·cm^2 at 21 days before decreasing to 12.840 Ω·cm^2 at 28 days. Similarly, R_{ct} for the blank sample fluctuates between

https://doi.org/10.1021/acsomega.3c10240
ACS Omega 2024, 9, 27945−27962

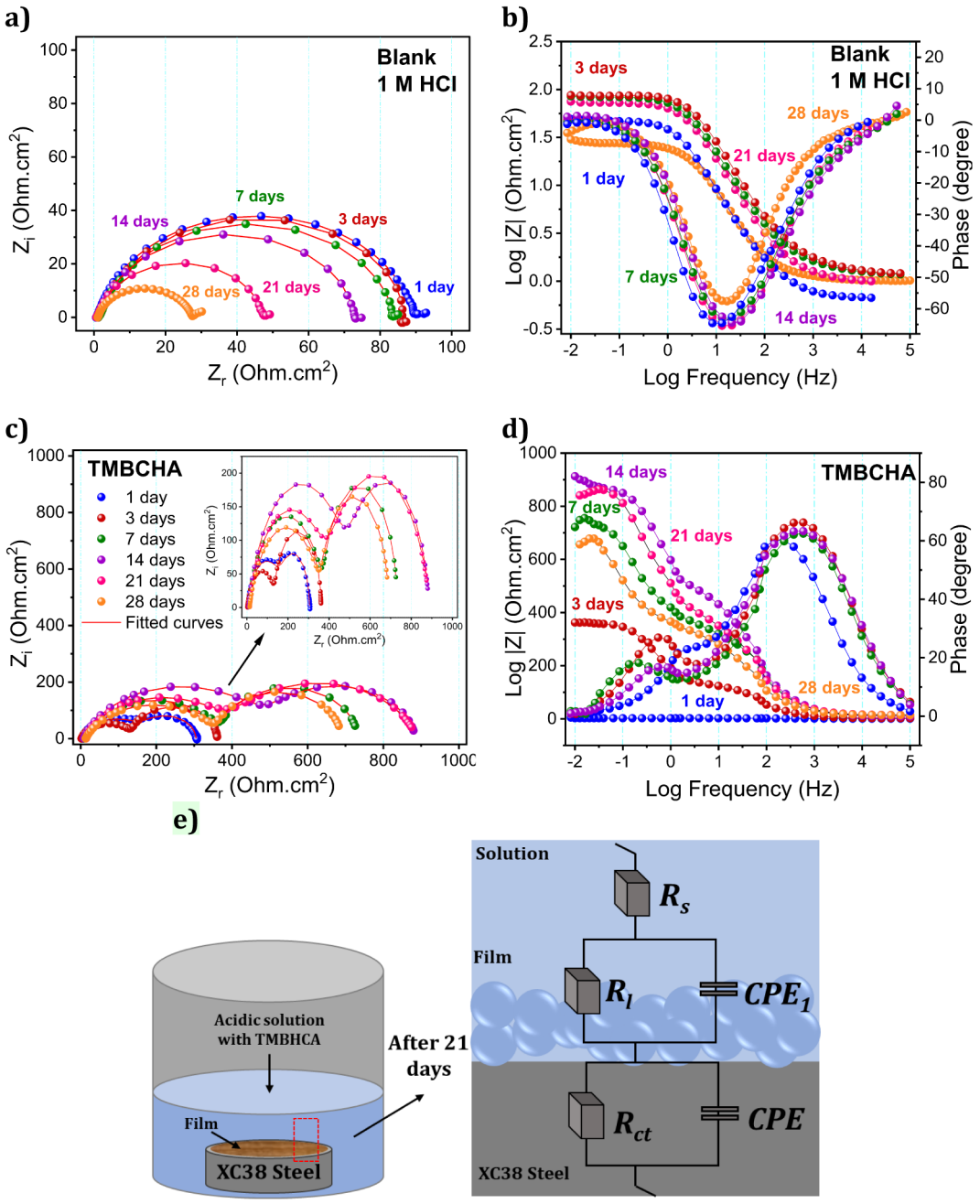

Figure 8. Nyquist and bode plots for XC38 carbon steel in 1 M HCl without (a and b) and with 200 ppm of TMBCHA (c and d) at various immersion durations and proposed electrical equivalent circuit model for fitting impedance data points and its significance on the corrosion of XC38 steel with TMBHCA inhibitor after 21 days (e).

87.84 Ω·cm^2 and 26.68 Ω·cm^2, while for TMBCHA-treated samples, R_{ct} ranges from 160.2 Ω·cm^2 to 528.9 Ω·cm^2. These variations highlight the dynamic changes in the corrosion inhibition mechanism with varying immersion durations, confirming its pivotal role in augmenting the adsorptive interaction between the inhibitor molecules and the steel surface, concluding in significantly enhanced corrosion protection.

3.3. Adsorption Isotherm Analysis. The exploration of how corrosion inhibitors interact with metal surfaces' active sites is significantly advanced by leveraging established adsorption isotherm models, such as those proposed by Freundlich, Temkin, Flory–Huggins, Frumkin, and Langmuir.[71,72] These models provide a robust theoretical foundation for delving into the mechanisms through which corrosion inhibitors adsorb onto metal surfaces.

In this study, the adsorption dynamics are methodically characterized through the application of three distinguished isotherm models:[73,74]

$$\text{Langmuir:} \quad \frac{\theta}{(1-\theta)} = b \cdot C_{eq} \tag{12}$$

$$\text{Tamkin mode:} \quad \exp(-2a\theta) = K \cdot C_{eq} \tag{13}$$

$$\text{Frumkin mode:} \quad \left(\frac{\theta}{1-\theta}\right)\exp(-2a\theta) = K \cdot C_{eq} \tag{14}$$

https://doi.org/10.1021/acsomega.3c10240
ACS Omega 2024, 9, 27945−27962

Table 4. Electrochemical Impedance Spectroscopy Characteristics for the Carbon Steel Corrosion in 1 M HCl without and with 200 ppm of TMBCHA at Various Immersion Durations

		CPE			CPE_1						
time (days)	R_s ($\Omega \cdot cm^2$)	($F \cdot s^1(a^{-1})$)	n	R_1 ($\Omega \cdot cm^2$)	($F \cdot s^1(a^{-1})$)	n'	R_{ct} ($\Omega \cdot cm^2$)	x^2	$x^2/\|Z\|$	$X/N^{1/2}$	EI (%)
Blank											
1 day	1.063	1.26×10^{-03}	0.909	87.84	-	-	-	64.12	7.7	0.985	-
3 days	1.975	7.19×10^{-04}	0.909	85.19	-	-	-	35.41	2.68	1.086	-
7 days	1.816	1.02×10^{-03}	0.892	82.19	-	-	-	8.23	1.973	0.754	-
14 days	1.454	1.14×10^{-03}	0.907	71.62	-	-	-	16.7	1.126	0.746	-
21 days	0.996	2.42×10^{-03}	0.906	46.53	-	-	-	4.583	1.573	0.39	-
28 days	1.042	2.98×10^{-03}	0.861	26.68	-	-	-	5.318	0.061	0.286	-
TMBCHA											
1 day	5.988	7.48×10^{-05}	0.846	160.2	9.22×10^{-04}	0.974	138.7	911.2	0.114	4.963	45.16
3 days	2.563	1.90×10^{-03}	0.999	222.9	6.61×10^{-05}	0.835	135.5	1276	0.172	5.578	61.78
7 days	8.753	2.26×10^{-03}	0.981	355.1	2.79×10^{-05}	0.805	367.4	12376	0.18	18.29	76.85
14 days	8.276	1.03×10^{-03}	0.93	385.1	2.81×10^{-05}	0.796	491.9	4573	0.151	11.12	81.40
21 days	13.730	1.19×10^{-03}	0.794	528.9	3.15×10^{-05}	0.803	369.8	6027	0.112	12.76	91.20
28 days	12.840	6.29×10^{-05}	0.75	352.8	5.31×10^{-03}	0.994	323.8	7819	0.118	13.98	**92.43**

The parameters b, K, a, and α represent the adsorption coefficient, the equilibrium adsorption constant, and the molecular interaction parameter, respectively.

These isotherms are instrumental in defining the distinctions of inhibitor−metal surface interactions, offering insights into the extent of surface coverage (θ), which is corroborated by gravimetric analysis as defined by the relation:

$$\theta = \frac{\text{IE (\%)}}{100} \tag{15}$$

The observed results indicate that mild steel can significantly retard the corrosion rate in the HCl medium by creating a corrosion−inhibitor coating on its surface. To facilitate the adhesion of corrosion inhibitor molecules to mild steel surfaces, water molecules must first be displaced,[27,75] as expressed in eq 16:

$$\text{Inh}_{(\text{solution})} + m\text{H}_2\text{O}_{(\text{adsorption})} \leftrightarrow \text{Inh}_{(\text{adsorption})} + \text{H}_2\text{O}_{(\text{solution})} \tag{16}$$

Here, $\text{Inh}_{(\text{solution})}$ and $\text{H}_2\text{O}_{(\text{solution})}$ represent the inhibitor and water molecules in the solution, respectively, and $\text{Inh}_{(\text{adsorption})}$ and $\text{H}_2\text{O}_{(\text{adsorption})}$ signify the inhibitor and H_2O molecules adsorbed onto surfaces, respectively, with m defining the number of H_2O molecules displaced by the inhibitor molecules.

Diverse isotherms were employed to interpret experimental data, with the Langmuir adsorption isotherm model demonstrating the most favorable alignment. This model facilitated the quantification of θ across varying concentrations of TMBCHA in 1 M HCl, aiming to elucidate the adsorption behavior. Figure 9 illustrates C_{inh}/θ in relation to C_{inh} for varying concentrations of TMBCHA, revealing linear correlations with coefficients (R^2) approaching unity and slopes near one. Such findings underscore the alignment of TMBCHA adsorption with the Langmuir model principles, where θ correlates directly with the inhibitor concentration as denoted in eq 17:

$$\frac{C}{\theta} = \frac{1}{K} + C \tag{17}$$

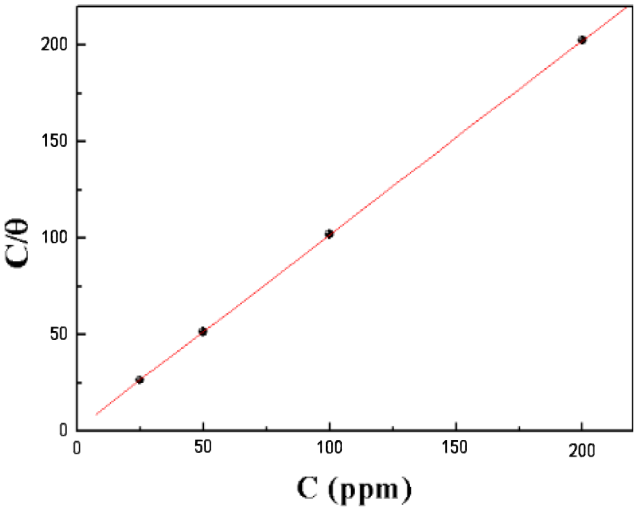

Figure 9. Langmuir isotherm model plots for XC38 carbon steel in 1 M HCl with different TMBCHA concentrations.

In Figure 9, the equilibrium constant for the adsorption process is represented by the symbol K, where C denotes the inhibitor concentration, and θ (calculated as E_{WL} %/100) represents the fraction of the metal surface covered by the inhibitor. This relationship between C, θ, and K not only facilitates a deeper understanding of the inhibitor's adsorptive behavior but also underscores the Langmuir isotherm model's applicability in describing the interaction dynamics between the inhibitor and the metal surface. The use of K in this context yields critical insights into the adsorption process's efficacy, evidencing the inhibitor's capacity to establish a robust protective layer against corrosion on the metal interface.[76]

3.4. Surface Microscopic Observation. The investigation of material surfaces and the changes they undergo is essential in understanding their properties and modifications. SEM analysis stands as a widely utilized technique for scrutinizing surface characteristics. In the present study, SEM was employed to discover alterations in the surface properties of XC38, with and without TMBCHA corrosion inhibitor. Figure 10 displays the SEM images obtained during the investigation. Figure 10 presents SEM images of the XC38 surface after immersion for 24 h in 1 M HCl solution, both

https://doi.org/10.1021/acsomega.3c10240
ACS Omega 2024, 9, 27945−27962

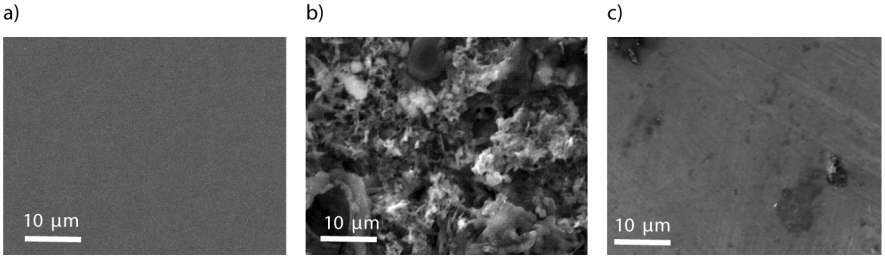

Figure 10. SEM images of (a) polished XC38 carbon steel, (b) XC38 carbon steel in 1 M HCl (blank), and (c) XC38 carbon steel with 200 ppm inhibitor after exposing for 24 h at ×10,000 magnification.

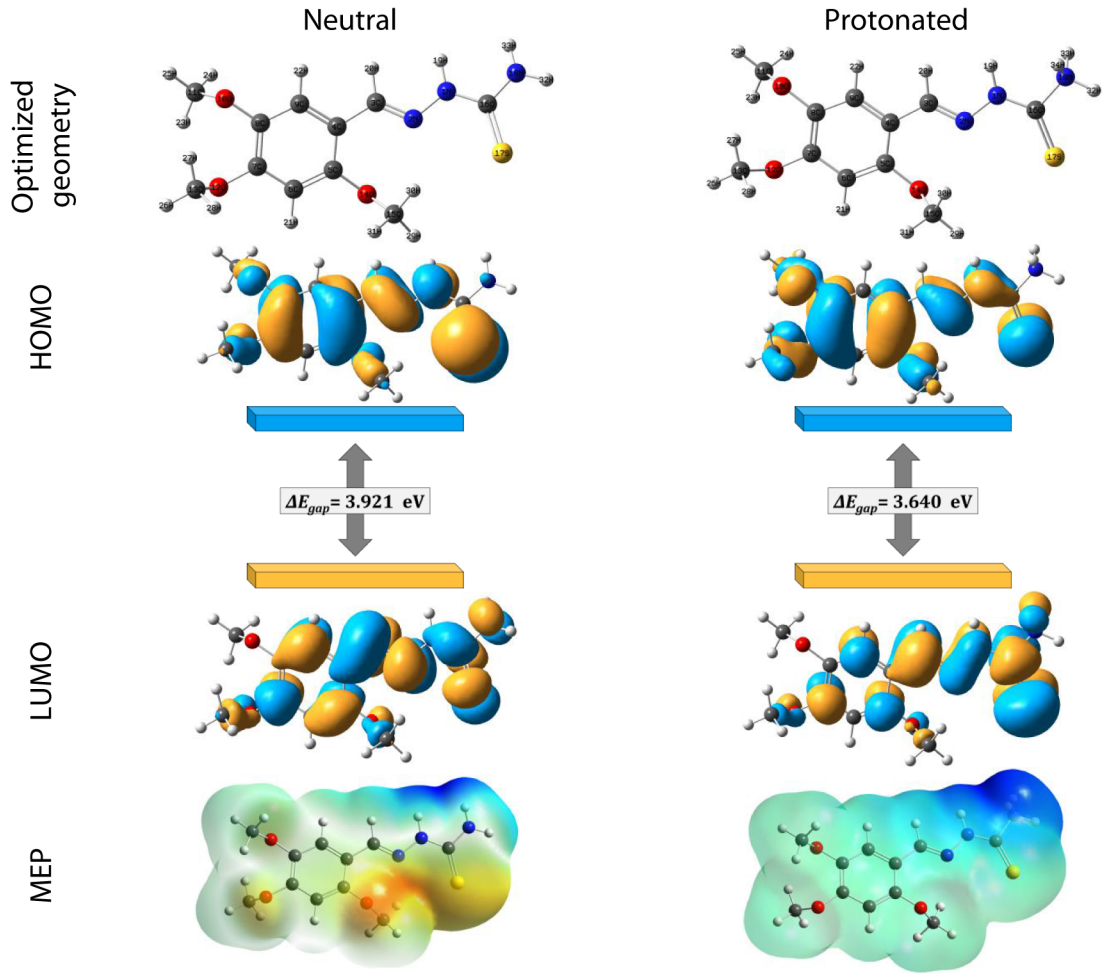

Figure 11. Optimized structures obtained viaquantum chemical computations, HOMO, LUMO orbitals, and MEP of neutral and protonated TMBHCA molecules.

without and with 200 ppm of TMBCHA. In Figure 10a, the SEM image reveals the polished XC38 carbon steel surface, which appears smooth, flat, and clean. This image serves as a reference for the initial state of the surface. In Figure 10b, the metal surface immersed in HCl appears highly damaged, exhibiting numerous pits and cracks indicative of extensive XC38 steel dissolution. However, in Figure 10c, the steel surface shows significant improvement with the accumulation of 200 ppm of TMBCHA in the corrosive medium. A protective inhibitive coating is visible, covering the XC38 carbon steel surface. This film acts to reduce metal dissolution, providing substantial corrosion prevention.[77] The SEM images are consistent with the findings derived from the previously discussed electrochemical measurements, providing additional support for the efficacy of the organic film in inhibiting corrosion.

3.5. Quantum Chemical Computations. *3.5.1. Global Chemical Reactivity.* Historically, the quest for novel corrosion inhibitors relied on modifying the structures of conventional inhibitors or empirical investigations.[78−81] However, there has been a recent shift toward employing quantum chemical methods, particularly DFT computation, to delve into the electronic and molecular properties of inhibitors.[82,83] DFT calculations, known for their accuracy, robustness, and utility, provide a valuable avenue for comprehending inhibitor properties, delineating their behavior, and facilitating the design and analysis of innovative inhibitors. In this study, DFT-based calculations are employed to

https://doi.org/10.1021/acsomega.3c10240
ACS Omega 2024, 9, 27945−27962

investigate the relationship between the corrosion behavior and the structural characteristics of TMBHCA. Figure 11 illustrates the optimized structures of TMBHCA in its neutral state, alongside the corresponding protonated highest occupied molecular orbital (HOMO) and lowest unoccupied molecular orbital (LUMO) electron density distributions. These visualizations offer valuable understandings into the electronic characteristics and reactivity of TMBHCA.

The analysis of frontier molecular orbitals (FMOs) is pivotal in elucidating interactions between molecules and other species. Specifically, the energies of the E_{HOMO} and E_{LUMO} provide insights into the strong inclination of inhibitor compounds to either donate or accept electrons from the metal surface. Summarized in Table 5, the obtained results

Table 5. Calculated Reactivity Indices Using DFT Functional for Various Parameters

parameter	neutral	protonated
E_T (eV)	−1215.967	−1216.405
E_{HOMO} (eV)	−5.455	−6.464
E_{LUMO} (eV)	−1.534	−2.824
energy gap (ΔE_{gap}, eV)	3.921	3.640
chemical potential (μ, eV) = $-\chi$	−3.495	−4.644
ionization potential (I, eV) = ($-E_{HOMO}$)	5.455	6.464
electron affinity (A, eV) = ($-E_{LUMO}$)	1.534	2.824
hardness (η, eV) = 0.5 * ($I - A$)	1.961	1.820
softness (σ, eV) = $1/\eta$	0.255	0.275
electronegativity (χ, eV) = ($I + A$)/2	3.495	4.644
global electrophilicity (ω, eV) = ($\mu * \mu$)/$\eta * 2$)	1.557	2.962

enable the calculation of reactivity indices. The energy gap, denoted by ΔE_{gap}, acts as an indicative parameter of the reactivity of inhibitor molecules to adsorption on metal surfaces. A smaller ΔE_{gap} signifies higher reactivity and enhanced efficiency of inhibitor adsorption, resulting in increased inhibition efficiency.[84,85] Moreover, the χ of the TMBHCA inhibitor molecule reflects its propensity to release electrons to accepting species. A higher χ value indicates a stronger electron-holding ability, while a lower value suggests a greater likelihood of electron donation. Additionally, the η and σ values serve as valuable indicators of chemical reactivity and inhibition ability.[23,86] A lower η value and higher σ value correspond to higher reactivity and increased inhibition ability, respectively. The molecular ω describes the electrophilic power of the molecule structure, with a higher ω value signifying a superior capacity of the molecule to accept electrons.[87−90]

Comprehending the protonation state of TMBHCA inhibitor molecules holds paramount importance, as it profoundly influences their reactivity and efficacy in corrosion inhibition. In aqueous solutions, the prevailing protonated state of inhibitors is attributed to the presence of hydrogen ions (H^+). The protonation process enhances the interaction of TMBHCA inhibitor compounds with the metal surface, thereby augmenting their corrosion inhibitory capabilities. A comprehensive examination of both protonated and non-protonated states of TMBHCA molecules provides a nuanced understanding of their reactivity and effectiveness in diverse environmental conditions.[88] Understanding this information is crucial for advancing the development of corrosion inhibitors that demonstrate enhanced efficiency and effectiveness across a spectrum of industrial applications.

Additionally, scientific investigations consistently emphasize that the adsorption of inhibitors onto metallic surfaces can be attributed to donor−acceptor interactions. This is notably evident in the interaction between the π electrons of heterocyclic compounds and the unoccupied d orbitals of metal surface atoms. These interactions play a crucial role in the development of a protective layer on the metal surface, thereby enhancing corrosion inhibition. Simultaneously, the spatial distribution of electrons, controlled by the HOMO, dictates electrophilic attacks, which tend to occur at atomic sites with a high density of HOMO orbitals. Figure 11 offers insightful visualizations of this phenomenon, with the blue and orange areas representing FMOs of opposite phases. The blue color signifies the positive phase, while the orange color denotes the negative phase. Notably, the distributions of the LUMO and HOMO orbitals are similar in both neutral and protonated states. Furthermore, the HOMO orbital distribution spans the conjugate part of the molecule and all heteroatoms (O, N, and S), indicating a widespread distribution of π-electrons throughout the entire molecule. This distinction underscores the primary adsorption sites of these substances. The presence of additional adsorption sites has the potential to influence the formation of a flat surface on iron metal, thereby affecting the adsorption behavior and corrosion inhibition properties of TMBHCA molecules.

Furthermore, molecular electrostatic potential (MEP) provides a visual representation of the electrostatic distribution within a molecule, aiding in the identification of binding sites and interactions with neighboring molecules. In Figure 11, the MEP profile is presented through a color-coded map. Regions with maximum negative potential, promoting electrophilic attack, are visualized in red. Conversely, areas with significant positive potential, favoring nucleophilic attack, are shown in blue, while the zero-potential region is indicated in green. The intensity, shape, and extent of positive, negative, and neutral electrostatic potentials are effectively conveyed through distinct color gradients, where the potential increases in the order red < orange < yellow < green < blue. As a results, from the MEP map presented in Figure 11, it is evident that the high electronic density suitable for electrophilic attack (yellow region) is proximate to the sulfur atom, whereas the green region corresponds to carbon and hydrogen. Notably, the protonated form of TMBHCA exhibits the highest potential, signifying a greater inclination for electrophilic and nucleophilic attacks. The red areas signify negative charges conducive to nucleophilic attack, indicating a high potential for covalent bond formation with iron d orbitals. In the protonated form, the blue regions suggest electron-receiving capabilities of the metal. These findings offer valuable insights into the molecular structure and characteristics of TMBHCA, emphasizing its effective inhibitory capacity against corrosion.

3.5.2. Local Chemical Reactivity. To identify the active sites responsible for nucleophilic and electrophilic interactions within TMBHCA in both its neutral and protonated forms, we conducted calculations involving Fukui indices. Fukui index is one of the largest used reactivity parameters to explain chemical reactivity of an electrophilic and nucleophilic attack site in a molecule. The two types of Fukui functions f_k^+ and f_k^- are used to characterize the electrophilic and nucleophilic powers of atoms. The most reactive site of the molecule is probably the one with the highest value of the Fukui function.The atom condensed form of Fukui functions was

https://doi.org/10.1021/acsomega.3c10240
ACS Omega 2024, 9, 27945−27962

proposed by Yang et al.[91] The forms of three Fukui functions' types are defined as follows:

$$f_k^+ = [q_k(N+1) - q_k(N)] \quad \text{Nucleophilic attack}$$

$$f_k^- = [q_k(N) - q_k(N-1)] \quad \text{Electrophilic attack}$$

$$f_k^0 = \frac{[q_k(N+1) - q_k(N-1)]}{2} \quad \text{free - radical attack}$$

Here, f_k, $q_k(N)$, $q_k(N+1)$, and $q_k(N-1)$ are, respectively, the Fukui function corresponding to site k, the popular electronics of the k atom in the neutral molecule, in the anionic molecule, and in the cationic molecule.

The local electrophilicity ω_k^+ can be calculated from the global electrophilicity index (ω) and the electrophilic Fukui index (f^+) according to the following equation:

$$\omega_k^+ = \omega f^+ \tag{18}$$

The results of Fukui and local electrophilicity indices are summarized in Table 6.

Table 6. Local Reactivity Parametersof Studied Molecule

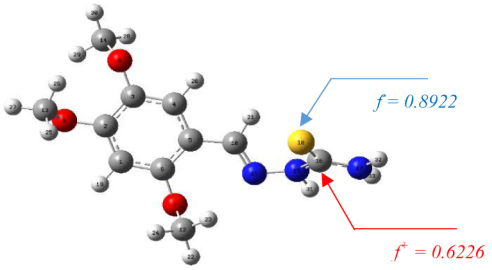

atoms	f^-	f^+	ω^+	ω^-
N15	0.0103	0.0109	0.0098	0.0092
C16	0.0790	**0.6226**	**0.5586**	0.0709
N17	0.0091	0.0115	0.0103	0.0082
S18	**0.8922**	0.3533	0.3170	**0.8004**
H33	0.0084	0.0002	0.0002	0.0076

The values of f^+ and ω^+ indicate that the carbon atom (C16) has the highest values; thus, it is the most susceptible to attack by a nucleophilic reagent. On the other hand, the highest values of f^- and ω^- are those of the sulfur atom (S16), suggesting that this atom is susceptible to electrophilic attack. We also remark that the two nitrogens (N15) and (N17) have acceptable values of f^+, f^-, ω^+, and ω^-, so they can contribute to electrophilic or nucleophilic attack.

3.5.3. Noncovalent Interaction Study. The NCI concept stands as an advanced computational approach extensively performed for unraveling intermolecular interactions and depicting weak forces in molecular structures. This theory utilizes visualization indicators based on density and relevant metrics, color-coded to reflect strength according to RDG values at low densities. The NCI method involves evaluating electron density (ρ) and multiplying it by the sign of the second-highest eigenvalue (λ_2) of the Hessian matrix of the electron density at each point on the isosurface. This product, represented as $(\lambda_2) \times \rho$, indicates whether intermolecular forces are attractive or repulsive. A negative sign of the product $(\lambda_2) \times \rho$ denotes primarily attractive interactions, often associated with hydrogen bond formation. Conversely, a positive sign indicates the presence of steric repulsion or nonbonding interactions.[92,93] Figure 12 displays the NCI-RDG plots derived from the density analysis of the investigated TMBHCA compound. The plots unveil various intermolecular interactions in both the neutral and protonated states of the TMBHCA molecule. HB, VDW, and steric repulsive interactions are visualized in blue, green, and red, respectively. The RDG isovalue within the range of −0.035 to 0.020 au and the sign of $(\lambda_2) \times \rho$ signifies the strength and nature of these interactions. Electron clouds within these regions exhibit stability through interactions with appropriate acceptors. The scatter diagram, depicted in red, illustrates that the interaction among the TMBHCA and the targeted metal surfaces effectively minimizes steric-repellent interactions. This interaction is facilitated by N and S heteroatoms, as well as methoxy or aromatic groups within the corrosion inhibitory substance's chemical structure. These properties foster the creation of an effective adsorption coating layer, reinforcing interactions with the metal surface.

Therefore, this consistent observation is in line with the insights derived from our comprehensive analyses, encompassing FMO, MEP, and Fukui analyses. The amalgamation of these analyses serves to underscore the nuanced reactivity and bonding characteristics inherent in TMBHCA molecules. By delving into the electronic structure through FMO, the spatial distribution of electron density via MEP, and the site-specific reactivity using Fukui indices, we gain a holistic understanding of the molecular attributes influencing the inhibitory mechanism. Meanwhile, this enhanced understanding of the inhibitory mechanism, derived from a comprehensive analysis of these quantum chemical parameters, enriches our comprehension of how TMBHCA effectively safeguards metal surfaces from corrosion. It is essential to note that while these quantum chemical parameters provide valuable theoretical insights, their direct correlation with experimental inhibition efficiencies has been a subject of recent criticism in the literature.[76] As such, the focus on DFT calculations in this study was intended to confirm the inhibition potential of TMBHCA and establish correlations with experimental inhibition efficiencies.

3.6. Proposed Inhibitory Mechanism. Exploring the inhibition mechanism at the interface of XC38 carbon steel and HCl has been pivotal in deciphering the intricate processes that underlie corrosion inhibition. This investigative approach, guided by a blend of experimental analyses and computational insights, has provided valuable understandings into the underlying corrosion inhibition mechanisms of TMBHCA molecule. The elucidation of the inhibition mechanism in HCl is attainable through an understanding of the adsorption mode. The adsorption process is altered by the charge on the metal surface, the nature of interaction with the metal surface, and the molecular structure of the inhibitor molecules.[94]

In this study, we propose the adsorption mechanism of TMBHCA. Initially, TMBHCA undergoes protonation in the presence of HCl, and the liberated Cl^- anion adheres to the XC38 metal surface, potentially influencing the nucleophilicity of other heteroatoms (N═C, NH, and S═) (Figure 13 a). In this scenario, the charge on the metal surface may influence the adsorption of Cl^- ions. However, we acknowledge that we did not directly determine the excess surface charge, and it is crucial to note that our conclusion about the positive charge on the metal surface enhancing Cl^- ion adsorption is based on the proposed mechanism and may require further investigation. To strengthen the validity of this proposed

https://doi.org/10.1021/acsomega.3c10240
ACS Omega 2024, 9, 27945−27962

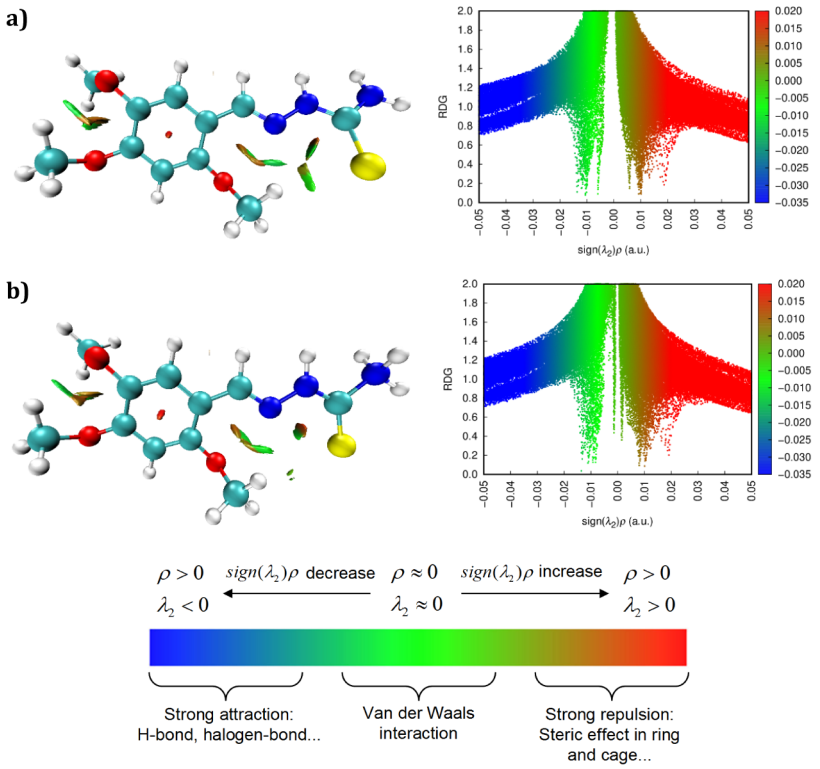

Figure 12. RDG scatter plots (left) and NCI plots (right) isosurface (s = 0.5 au) of (a) neutral and (b) protonated TMBHCA.

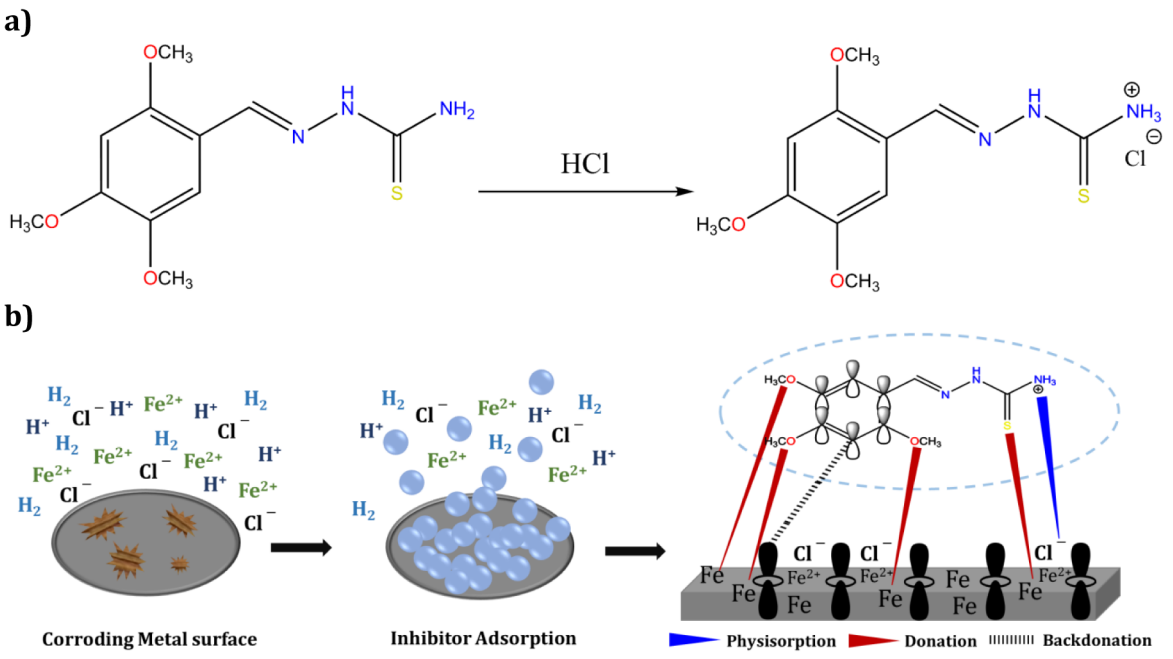

Figure 13. (a) TMBHCA molecule protonation in the presence of HCl and (b) proposed inhibition mechanism for the XC38 surface employing TMBHCA.

mechanism, future work may involve direct determination of the excess surface charge to ascertain the nature of the metal surface charge and its impact on Cl^- ion adsorption.[95] This additional step would provide more concrete evidence and further insight into the adsorption process, enhancing the overall understanding of the corrosion inhibition mechanism of TMBHCA.[96−99] Figure 13 b offers a schematic representation of diverse adsorption modes at the metal−acid interface.

In addition to physical adsorption, neutral inhibitors can chemically adsorb onto the XC38 carbon steel surface through direct electron sharing, based on donor−acceptor interactions between the π-electrons of the heterocyclic ring and the unoccupied d-orbitals of surface iron atoms. Iron tends to coordinate with the inhibitor heteroatoms, creating an adsorptive film. Whether through physical or chemical adsorption, or a combination of both, the establishment of

https://doi.org/10.1021/acsomega.3c10240
ACS Omega 2024, 9, 27945−27962

an adsorptive film on corroding steels leads to a reduction in the corrosion rate. As the inhibitor concentration increases, the adsorptive film extends to cover larger surface areas, contributing to an amplified inhibition efficiency.

In summary, this enriched understanding of the inhibitory mechanism is derived from a thorough analysis that integrates theoretical and experimental aspects. This holistic approach not only recognizes the inherent limitations of current methodologies but also acknowledges the ongoing debates within the field of corrosion inhibition. By bridging theoretical insights with experimental observations, this study actively contributes to the evolving discourse on the evaluation of corrosion inhibitors. Looking ahead, further additional analyses, including molecular dynamics simulations, are essential for advancing our understanding and providing a more comprehensive insight into the complex interactions between the metal surface and the inhibitor. These simulations hold promise for providing deeper insights into the intricacies of the adsorption/interaction energies between the metal surface and the inhibitor, further advancing our understanding of corrosion inhibition mechanisms.

3.7. Conclusion. In summary, the studied compound demonstrated significant effectiveness as an inhibitory corrosion inhibitor for XC38 steel under acidic medium, showing an increasing trend in inhibition efficiency with elevated TMCBHA concentration. The comprehensive array of results allows for the following key conclusions:

- Gravimetric analysis revealed that TMCBHA effectively inhibited XC38 steel corrosion in a 1 M HCl medium, reaching an impressive inhibition effectiveness up to 98%. The detected increase in inhibition efficiency with rising inhibitor concentrations was consistent with weight loss examinations.
- Potentiodynamic polarization measurements indicated a reduction in corrosion currents upon the addition of TMCBHA, influencing both anodic and cathodic processes. TMCBHA displayed characteristics of a mixed-type inhibitor, with Tafel polarization values supporting an inhibition effectiveness of 93%.
- Electrochemical impedance spectroscopy (EIS) measurements demonstrated a rise in charge transfer resistance (R_{ct}) and a reduction in double-layer capacitance (C_{dl}) in the presence of inhibitors, indicating the adsorption of TMCBHA inhibitor on the XC38 carbon steel surface. These findings propose that the TMCBHA molecules interact with the surface of metal, effectively blocking active sites and contributing to the development of corrosion protection.
- Scanning electron microscopy (SEM) images performed a visual confirmation of the creation of a protecting coating composed of TMCBHA inhibitors on XC38 carbon steel surface.
- The immersion test conducted over 28 days under acid cleaning conditions showcased the effectiveness of the considered inhibitor. The evaluation revealed a substantial rise in inhibition effectiveness from 45.16% to 92.43% at 200 ppm as the immersion period extended from 1 day to 28 days. This enhancement is ascribed to the heightened adsorption of TMCBHA molecules on the XC38 surface, ensuring more comprehensive coverage and effective protection against corrosion.
- Quantum chemical investigations provided intricate insights into the donor−acceptor interaction mode, affirming the adsorption capability of TMCBHA on the XC38 surface. The horizontal alignment of active species within TMCBHA, displacing preadsorbed water molecules, enhances corrosion resistance.

In conclusion, the exhaustive combination of experimental and theoretical analyses presented in this study collectively emphasizes the considerable promise of TMCBHA as a potent corrosion inhibitor. The comprehensive insights gained not only deepen our understanding of the inhibitory mechanisms at play but also pave the way for the prospective application of TMCBHA in diverse industrial settings. This integrative approach, considering both theoretical and experimental aspects, underscores the potential significance of TMCBHA as a corrosion inhibitor, offering valuable contributions to the ongoing discourse in corrosion science. Furthermore, additional analyses, including molecular dynamics simulations, are essential for a more thorough exploration of the intricate interactions that govern the effectiveness of TMCBHA, thus providing avenues for continued research and development in corrosion inhibition.

AUTHOR INFORMATION

Corresponding Authors

Hana Ferkous − *Département de Technologie, Université20 Août 1955-Skikda, Skikda 21000, Algeria; Laboratoire de Génie Mécanique et Matériaux, Faculté de Technologie, Université 20 Août 1955-Skikda, Skikda 21000, Algeria*; Email: h.ferkous@univ-skikda.dz

Yacine Benguerba − *Laboratoire de Biopharmacie Et Pharmacotechnie (LBPT), Ferhat Abbas Setif 1 University, Setif 19000, Algeria*; orcid.org/0000-0002-8251-9724; Email: benguerbayacine@yahoo.fr

Authors

Nadia Mouats − *Département de Technologie, Université20 Août 1955-Skikda, Skikda 21000, Algeria*

Souad Djellali − *Laboratoire de Physico-Chimie des Hauts Polymères (LPCHP), Faculty of Technology, University of Ferhat Abbas Setif 1, Setif 19000, Algeria*; orcid.org/0000-0002-0205-4649

Amel Sedik − *Scientific and Technical Research Center in Physico-chemical Analysis. BP 384, Tipaza RP 42004, Algeria; Nanomaterials, corrosion and surface treatment laboratory (LNMCT), BP 12, Badji Mokhtar University, Annaba 23000, Algeria*

Amel Delimi − *Département de Technologie, Université20 Août 1955-Skikda, Skikda 21000, Algeria; Laboratoire de Génie Mécanique et Matériaux, Faculté de Technologie, Université 20 Août 1955-Skikda, Skikda 21000, Algeria*

Abir Boublia − *Laboratoire de Physico-Chimie des Hauts Polymères (LPCHP), Faculty of Technology, University of Ferhat Abbas Setif 1, Setif 19000, Algeria*; orcid.org/0000-0003-1669-4951

Khadidja Otmane Rachedi − *Laboratory of Applied Organic Chemistry LCOA, Synthesis of biomolecules and molecular modelingGroup, Badji -Mokhtar - Annaba University, Annaba 23000, Algeria*

Malika Berredjem − *Laboratory of Applied Organic Chemistry LCOA, Synthesis of biomolecules and molecular modelingGroup, Badji -Mokhtar - Annaba University, Annaba 23000, Algeria*

https://doi.org/10.1021/acsomega.3c10240
ACS Omega 2024, 9, 27945−27962

Alaaddin Çukurovali − *Department of Chemistry, Faculty of Sciences, Firat University, Elazĭ 23119, Turkey*
Manawwer Alam − *Department of Chemistry, College of Science, King Saud University, Riyadh 11451, Saudi Arabia;* orcid.org/0000-0001-9540-8532
Barbara Ernsti − *Laboratoire de Reconnaissance et Procédés de Séparation Moléculaire (RePSeM), Université de Strasbourg, CNRS, IPHC UMR 7178, Strasbourg F-67000, France*

Complete contact information is available at: https://pubs.acs.org/10.1021/acsomega.3c10240

Notes

The authors declare no competing financial interest.

■ ACKNOWLEDGMENTS

The authors gratefully acknowledge the funding from Researchers Supporting laboratoire de Génie mécanique et Matériaux, Faculté de Technologie, University 20 Août 1955-Skikda, Skikda, 21000, Algeria, and the Ministry of Higher Education and Scientific Research, Ferhat ABBAS Setif 1 University, the Directorate General for Scientific Research and Technological Development (DGRSDT), Algeria. The authors are thankful to the Researchers Supporting Project (RSP2024R113), King Saud University, Riyadh, Saudi Arabia.

■ REFERENCES

(1) Kumar, R.; Chahal, S.; Dahiya, S.; Dahiya, N.; Kumar, S.; Lata, S. Experimental and Theoretical Approach to Exploit the Corrosion Inhibition Activity of 3-Formyl Chromone Derivatives on Mild Steel in 1 m H2SO4. *Corros. Rev.* **2017**, *35* (2), 95−110.
(2) Prabhu, D.; Padmalatha, R. Studies of Corrosion of Aluminium and 6063 Aluminium Alloy in Phosphoric Acid Medium. *Int. J. ChemTech Res.* **2013**, *5* (6), 2690−2705.
(3) Bowman, E.; Jacobson, G.; Koch, G.; Varney, J.; Thopson, N.; Moghissi, O.; Gould, M.; Payer, J. *International Measures of Prevention, Application, and Economics of Corrosion Technologies*. NACE International, 2016.
(4) Sedik, A.; Lerari, D.; Salci, A.; Athmani, S.; Bachari, K.; Gecibesler, İ. H.; Solmaz, R. Dardagan Fruit Extract as Eco-Friendly Corrosion Inhibitor for Mild Steel in 1 M HCl: Electrochemical and Surface Morphological Studies. *J. Taiwan Inst. Chem. Eng.* **2020**, *107*, 189−200.
(5) Heakal, F. E.-T.; Deyab, M. A.; Osman, M. M.; Elkholy, A. E. Performance of Centaurea Cyanus Aqueous Extract towards Corrosion Mitigation of Carbon Steel in Saline Formation Water. *Desalination* **2018**, *425*, 111−122.
(6) Gabsi, M.; Ferkous, H.; Delimi, A.; Boublia, A.; Boulechfar, C.; Kahlouche, A.; Darwish, A. S.; Lemaoui, T.; Benguerba, Y. The Curious Case of Polyphenols as Green Corrosion Inhibitors: A Review on Their Extraction, Design, and Applications. *Environ. Sci. Pollut. Res.* **2023**, *30*, 1−25.
(7) Saraswat, V.; Kumari, R.; Yadav, M. Novel Carbon Dots as Efficient Green Corrosion Inhibitor for Mild Steel in HCl Solution: Electrochemical, Gravimetric and XPS Studies. *J. Phys. Chem. Solids* **2022**, *160*, 110341.
(8) Rahim, A. A.; Rocca, E.; Steinmetz, J.; Kassim, M. J. Inhibitive Action of Mangrove Tannins and Phosphoric Acid on Pre-Rusted Steel via Electrochemical Methods. *Corros. Sci.* **2008**, *50* (6), 1546−1550.
(9) El-Etre, A. Y.; Abdallah, M.; El-Tantawy, Z. E. Corrosion Inhibition of Some Metals Using Lawsonia Extract. *Corros. Sci.* **2005**, *47* (2), 385−395.
(10) Olasunkanmi, L. O.; Aniki, N. I.; Adekunle, A. S.; Durosinmi, L. M.; Durodola, S. S.; Wahab, O. O.; Ebenso, E. E. Investigating the Synergism of Some Hydrazinecarboxamides and Iodide Ions as Corrosion Inhibitor Formulations for Mild Steel in Hydrochloric Acid: Experimental and Computational Studies. *J. Mol. Liq.* **2021**, *343*, 117600.
(11) de Souza, F. S.; Spinelli, A. Caffeic Acid as a Green Corrosion Inhibitor for Mild Steel. *Corros. Sci.* **2009**, *51* (3), 642−649.
(12) Al-Otaibi, M. S.; Al-Mayouf, A. M.; Khan, M.; Mousa, A. A.; Al-Mazroa, S. A.; Alkhathlan, H. Z. Corrosion Inhibitory Action of Some Plant Extracts on the Corrosion of Mild Steel in Acidic Media. *Arab. J. Chem.* **2014**, *7* (3), 340−346.
(13) Zaferani, S. H.; Sharifi, M.; Zaarei, D.; Shishesaz, M. R. Application of Eco-Friendly Products as Corrosion Inhibitors for Metals in Acid Pickling Processes−A Review. *J. Environ. Chem. Eng.* **2013**, *1* (4), 652−657.
(14) Radjai, M.; Ferkous, H.; Zerroug, M.; Djellali, S.; Chaouch, M. A.; Hattabi, B.; Majdoub, H.; Boutahala, M. Methanolic Extract of Artemisia Herba Alba as Eco-Friendly Inhibitor of Carbon Steel Corrosion in 1m Hcl Media. *Adv. Sci. Technol. Innov.* **2018**, 1379−1381.
(15) Abd El-Lateef, H. M.; Soliman, K. A.; Tantawy, A. H. Novel Synthesized Schiff Base-Based Cationic Gemini Surfactants: Electrochemical Investigation, Theoretical Modeling and Applicability as Biodegradable Inhibitors for Mild Steel against Acidic Corrosion. *J. Mol. Liq.* **2017**, *232*, 478−498.
(16) Messali, M.; Larouj, M.; Lgaz, H.; Rezki, N.; Al-Blewi, F. F.; Aouad, M. R.; Chaouiki, A.; Salghi, R.; Chung, I.-M. A New Schiff Base Derivative as an Effective Corrosion Inhibitor for Mild Steel in Acidic Media: Experimental and Computer Simulations Studies. *J. Mol. Struct.* **2018**, *1168*, 39−48.
(17) Hasanov, R.; Sadıkŏlu, M.; Bilgiç, S. Electrochemical and Quantum Chemical Studies of Some Schiff Bases on the Corrosion of Steel in H2SO4 Solution. *Appl. Surf. Sci.* **2007**, *253* (8), 3913−3921.
(18) Altunbą¸ahin, E.; Tezcan, F.; Solmaz, R.; Kardą, G. Inhibitive Effect of 4-Amino-N-Benzylidene-Benzamide Schiff Base on Mild Steel Corrosion in HCl Solution. *J. Adhes. Sci. Technol.* **2020**, *34* (2), 135−152.
(19) Al-Sabagh, A. M.; Abd-El-Bary, H. M.; El-Ghazawy, R. A.; Mishrif, M. R.; Hussein, B. M. Corrosion Inhibition Efficiency of Linear Alkyl Benzene Derivatives for Carbon Steel Pipelines in 1M HCl. *Egypt. J. Pet.* **2011**, *20* (2), 33−45.
(20) Bouayed, M.; Rabaa, H.; Srhiri, A.; Saillard, J.-Y.; Bachir, A. B.; Le Beuze, A. Experimental and Theoretical Study of Organic Corrosion Inhibitors on Iron in Acidic Medium. *Corros. Sci.* **1998**, *41* (3), 501−517.
(21) Senthilkumar, G.; Umarani, C.; Ramachandran, A. Investigation on Corrosion Inhibition Effect of N-[4-(1, 3-Benzo [d] Thiazol-2-Ylcarbamoyl) Phenyl] Quinoline-6-Carboxamide as a Novel Organic Inhibitor on Mild Steel in 1N HCl at Different Temperatures: Experimental and Theoretical Study. *J. Indian Chem. Soc.* **2021**, *98* (6), 100079.
(22) Asadi, N.; Ramezanzadeh, M.; Bahlakeh, G.; Ramezanzadeh, B. Utilizing Lemon Balm Extract as an Effective Green Corrosion Inhibitor for Mild Steel in 1M HCl Solution: A Detailed Experimental, Molecular Dynamics, Monte Carlo and Quantum Mechanics Study. *J. Taiwan Inst. Chem. Eng.* **2019**, *95*, 252−272.
(23) Moumeni, O.; Mehri, M.; Kerkour, R.; Boublia, A.; Mihoub, F.; Rebai, K.; Khan, A. A.; Erto, A.; Darwish, A. S.; Lemaoui, T.; et al. Experimental and Detailed DFT/MD Simulation of α-Aminophosphonates as Promising Corrosion Inhibitor for XC48 Carbon Steel in HCl Environment. *J. Taiwan Inst. Chem. Eng.* **2023**, *147* (May), 104918.
(24) Boulechfar, C.; Ferkous, H.; Boufas, S.; Berredjem, M.; Delimi, A.; Djellali, S.; Djedouani, A.; Bahadi, R.; Laamari, S.; Yadav, K. K.; et al. Synthesis, Electrochemical, and Quantum Chemical Studies of Some Metal Complexes: Mn(II), Co(II), and Zn(II) with 2-Furaldehyde Semicarbazone. *J. Mol. Struct.* **2023**, *1271*, 134007.
(25) Liu, X.; Manzur, C.; Novoa, N.; Celedón, S.; Carrillo, D.; Hamon, J.-R. Multidentate Unsymmetrically-Substituted Schiff Bases and Their Metal Complexes: Synthesis, Functional Materials Properties, and Applications to Catalysis. *Coord. Chem. Rev.* **2018**, *357*, 144−172.

(26) Sakthivel, A.; Jeyasubramanian, K.; Thangagiri, B.; Raja, J. D. Recent Advances in Schiff Base Metal Complexes Derived from 4-Aminoantipyrine Derivatives and Their Potential Applications. *J. Mol. Struct.* **2020**, *1222*, 128885.
(27) Li, X.-L.; Xie, B.; Feng, J.-S.; Lai, C.; Bai, X.-X.; Li, T.; Zhang, D.-L.; Mou, W.-Y.; Wen, L.; Gu, Y.-T. 2-Pyridinecarboxaldehyde-Based Schiff Base as an Effective Corrosion Inhibitor for Mild Steel in HCl Medium: Experimental and Computational Studies. *J. Mol. Liq.* **2022**, *345*, 117032.
(28) Mahmood, A.; Mahmood, A.; Sarfraz, R. M.; Hussain, Z.; Afzal, A.; Boublia, A.; Bhutto, J. K.; Alreshidi, M. A.; Yadav, K. K.; Elboughdiri, N.; et al. Chitosan-Based Intelligent Polymeric Networks for Site-Specific Colon Medication Delivery: A Comprehensive Study on Controlled Release of Diloxanide Furoate and Network Formation Dynamics. *Int. J. Biol. Macromol.* **2024**, *255*, 128089.
(29) Verma, C.; Quraishi, M. A. Recent Progresses in Schiff Bases as Aqueous Phase Corrosion Inhibitors: Design and Applications. *Coord. Chem. Rev.* **2021**, *446*, 214105.
(30) Boulechfar, C.; Ferkous, H.; Delimi, A.; Djedouani, A.; Kahlouche, A.; Boublia, A.; Darwish, A. S.; Lemaoui, T.; Verma, R.; Benguerba, Y. Schiff Bases and Their Metal Complexes: A Review on the History, Synthesis, and Applications. *Inorg. Chem. Commun.* **2023**, *150*, 110451.
(31) Ashassi-Sorkhabi, H.; Shaabani, B.; Seifzadeh, D. Corrosion Inhibition of Mild Steel by Some Schiff Base Compounds in Hydrochloric Acid. *Appl. Surf. Sci.* **2005**, *239* (2), 154−164.
(32) Ma, L.; Li, W.; Zhu, S.; Wang, L.; Guan, S. Corrosion Inhibition of Schiff Bases for Mg-Zn-Y-Nd Alloy in Normal Saline: Experimental and Theoretical Investigations. *Corros. Sci.* **2021**, *184*, 109268.
(33) Boublia, A.; Guezzout, Z.; Haddaoui, N.; Badawi, M.; Darwish, A. S.; Lemaoui, T.; Lebouachera, S. E. I.; Yadav, K. K.; Alreshidi, M. A.; Algethami, J. S., et al. The Curious Case of Polyaniline-Graphene Nanocomposites: A Review on Their Application as Exceptionally Conductive and Gas Sensitive Materials. In *Critical Reviews in Solid State and Materials Sciences*; Taylor & Francis, 2023; pp. 125. .
(34) Nazir, U.; Akhter, Z.; Janjua, N. K.; Adeel Asghar, M.; Kanwal, S.; Butt, T. M.; Sani, A.; Liaqat, F.; Hussain, R.; Shah, F. U. Biferrocenyl Schiff Bases as Efficient Corrosion Inhibitors for an Aluminium Alloy in HCl Solution: A Combined Experimental and Theoretical Study. *RSC Adv.* **2020**, *10* (13), 7585−7599.
(35) Gürten, A. A.; Kelç, H.; Bayol, E.; Kandemirli, F. The Effect of Temperature and Concentration on the Inhibition of Acid Corrosion of Carbon Steel by Newly Synthesized Schiff Base. *J. Ind. Eng. Chem.* **2015**, *27*, 68−78.
(36) Frisch, M. J.; Trucks, G. W.; Schlegel, H. B.; Scuseria, G. E.; Robb, M. A.; Cheeseman, J. R.; Scalmani, G.; Barone, V.; Mennucci, B.; Petersson, G. *Gaussian 09, Revision D. 01*; Gaussian, Inc.: Wallingford CT, 2009.
(37) Boublia, A.; Lemaoui, T.; AlYammahi, J.; Darwish, A. S.; Ahmad, A.; Alam, M.; Banat, F.; Benguerba, Y.; AlNashef, I. M. Multitask Neural Network for Mapping the Glass Transition and Melting Temperature Space of Homo- and Co-Polyhydroxyalkanoates Using σ Profiles Molecular Inputs. *ACS Sustainable Chem. Eng.* **2023**, *11*, 208−227.
(38) Dennington, R.; Keith, T.; Millam, J. *GaussView, Version 5*, Informer Technologies, Inc., 2009.
(39) AlYammahi, J.; Darwish, A. S.; Lemaoui, T.; Boublia, A.; Benguerba, Y.; AlNashef, I. M.; Banat, F. Molecular Guide for Selecting Green Deep Eutectic Solvents with High Monosaccharide Solubility for Food Applications. *ACS Omega* **2023**, *8*, 26533.
(40) Lee, C.; Yang, W.; Parr, R. G. Development of the Colle-Salvetti Correlation-Energy Formula into a Functional of the Electron Density. *Phys. Rev. B* **1988**, *37* (2), 785−789.
(41) Frost, A. A.; Musulin, B. Density-Functional Thermochemistry III. The Role of Exact Exchange. *Hydrocarb. J. Chem. Phys.* **1953**, *21* (5648), 10−1063.
(42) Becke, A. D. Density-functional Thermochemistry III. The Role of Exact Exchange. *J. Chem. Phys.* **1993**, *98* (7), 5648−5652.
(43) Saha, S. K.; Murmu, M.; Murmu, N.; Banerjee, P. Benzothiazolylhydrazine Azomethine Derivatives for Efficient Corrosion Inhibition of Mild Steel in Acidic Environment: Integrated Experimental and Density Functional Theory Cum Molecular Dynamics Simulation Approach. *J. Mol. Liq.* **2022**, *364*, 120033.
(44) Johnson, E. R.; Keinan, S.; Mori-Sánchez, P.; Contreras-García, J.; Cohen, A. J.; Yang, W. Revealing Noncovalent Interactions. *J. Am. Chem. Soc.* **2010**, *132* (18), 6498−6506.
(45) Mandal, S.; Bej, S.; Banerjee, P. Insights into the Uses of Two Azine Decorated D10-MOFs for Corrosion Inhibition Application on Mild Steel Surface in Saline Medium: Experimental as Well as Theoretical Investigation. *J. Mol. Liq.* **2023**, *381*, 121789.
(46) Boutouil, A.; Laamari, M. R.; Elazhary, I.; Bahsis, L.; Anane, H.; Stiriba, S.-E. Towards a Deeper Understanding of the Inhibition Mechanism of a New 1,2,3-Triazole Derivative for Mild Steel Corrosion in the Hydrochloric Acid Solution Using Coupled Experimental and Theoretical Methods. *Mater. Chem. Phys.* **2020**, *241*, 122420.
(47) Lu, T.; Chen, F. Multiwfn: A Multifunctional Wavefunction Analyzer. *J. Comput. Chem.* **2012**, *33* (5), 580−592.
(48) Humphrey, W.; Dalke, A.; Schulten, K. VMD: Visual Molecular Dynamics. *J. Mol. Graphics* **1996**, *14* (1), 33−38.
(49) Williams, T.; Kelley, C.; Bröker, H. B.; Campbell, J.; Cunningham, R.; Denholm, D.; Elber, E.; Fearick, R.; Grammes, C.; Hart, L. *Gnuplot 4.5: an Interactive Plotting Program. 2011*; Gnuplot, 2017.
(50) Boulechfar, C.; Ferkous, H.; Delimi, A.; Berredjem, M.; Kahlouche, A.; Madaci, A.; Djellali, S.; Boufas, S.; Djedouani, A.; Errachid, A.; et al. Corrosion Inhibition of Schiff Base and Their Metal Complexes with [Mn (II), Co (II) and Zn (II)]: Experimental and Quantum Chemical Studies. *J. Mol. Liq.* **2023**, *378*, 121637.
(51) Popova, A.; Christov, M.; Vasilev, A. Mono-and Dicationic Benzothiazolic Quaternary Ammonium Bromides as Mild Steel Corrosion Inhibitors. Part II: Electrochemical Impedance and Polarisation Resistance Results. *Corros. Sci.* **2011**, *53* (5), 1770−1777.
(52) Solomon, M. M.; Umoren, S. A. In-Situ Preparation, Characterization and Anticorrosion Property of Polypropylene Glycol/Silver Nanoparticles Composite for Mild Steel Corrosion in Acid Solution. *J. Colloid Interface Sci.* **2016**, *462*, 29−41.
(53) Grillo, F.; Tee, D. W.; Francis, S. M.; Früchtl, H. A.; Richardson, N. V. Passivation of Copper: Benzotriazole Films on Cu (111). *J. Phys. Chem. C* **2014**, *118* (16), 8667−8675.
(54) Chang, T.; Leygraf, C.; Wallinder, I. O.; Jin, Y. Understanding the Barrier Layer Formed via Adding BTAH in Copper Film Electrodeposition. *J. Electrochem. Soc.* **2019**, *166* (2), D10.
(55) Lewandowski, B. R.; Lytle, D. A.; Garno, J. C. Nanoscale Investigation of the Impact of PH and Orthophosphate on the Corrosion of Copper Surfaces in Water. *Langmuir* **2010**, *26* (18), 14671−14679.
(56) Pareek, S.; Jain, D.; Hussain, S.; Biswas, A.; Shrivastava, R.; Parida, S. K.; Kisan, H. K.; Lgaz, H.; Chung, I.-M.; Behera, D. A New Insight into Corrosion Inhibition Mechanism of Copper in Aerated 3.5 Wt.% NaCl Solution by Eco-Friendly Imidazopyrimidine Dye: Experimental and Theoretical Approach. *Chem. Eng. J.* **2019**, *358*, 725−742.
(57) Fekri, M. H.; Omidali, F.; Alemnezhad, M. M.; Ghaffarinejad, A. Turnip Peel Extract as Green Corrosion Bio-Inhibitor for Copper in 3.5% NaCl Solution. *Mater. Chem. Phys.* **2022**, *286*, 126150.
(58) Jayaperumal, D. Effects of Alcohol-Based Inhibitors on Corrosion of Mild Steel in Hydrochloric Acid. *Mater. Chem. Phys.* **2010**, *119* (3), 478−484.
(59) Qiang, Y.; Li, H.; Lan, X. Self-Assembling Anchored Film Basing on Two Tetrazole Derivatives for Application to Protect Copper in Sulfuric Acid Environment. *J. Mater. Sci. Technol.* **2020**, *52*, 63−71.
(60) Xiong, S.; Liang, D.; Ba, Z.; Zhang, Z.; Luo, S. Adsorption Behavior of Thiadiazole Derivatives as Anticorrosion Additives on Copper Oxide Surface: Computational and Experimental Studies. *Appl. Surf. Sci.* **2019**, *492*, 399−406.

https://doi.org/10.1021/acsomega.3c10240
ACS Omega 2024, 9, 27945−27962

(61) Boulechfar, C.; Ferkous, H.; Djellali, S.; Amin, M. A.; Boufas, S.; Djedouani, A.; Delimi, A.; Ben Amor, Y.; Kumar Yadav, K.; Jeon, B.-H.; Benguerba, Y. DFT/Molecular Scale, MD Simulation and Assessment of the Eco-Friendly Anti-Corrosion Performance of a Novel Schiff Base on XC38 Carbon Steel in Acidic Medium. *J. Mol. Liq.* **2021**, *344*, 117874.
(62) Solmaz, R.; Dursun, Y. A.; ¸ahin, E. A.; Gecibesler, I. H.; Dörubą, M.; Tunç, M.; Çălayan, N.;¸ahin, I.; Dursun, I.; Bayındır, S.; et al. Bingöl Propolis Self-Assembled Monolayer Films: Preparation, Characterization and Application as Corrosion Inhibitors for Copper Protection in NaCl Environment. *Mater. Chem. Phys.* **2024**, *315*, 128956.
(63) Rahmouni, K.; Joiret, S.; Robbiola, L.; Srhiri, A.; Takenouti, H.; Vivier, V. Corrosion and Protection of High Leaded Tin Bronze Covered with Patina in NaHCO3+ Na2SO4 Solution Simulating Acid Rain in Urban Environment. *Bulg. Chem. Commun.* **2005**, *1*, 26−34.
(64) Zheludkevich, M. L.; Shchukin, D. G.; Yasakau, K. A.; Möhwald, H.; Ferreira, M. G. S. Anticorrosion Coatings with Self-Healing Effect Based on Nanocontainers Impregnated with Corrosion Inhibitor. *Chem. Mater.* **2007**, *19* (3), 402−411.
(65) Zuo, X.; Li, W.; Luo, W.; Zhang, X.; Qiang, Y.; Zhang, J.; Li, H.; Tan, B. Research of Lilium Brownii Leaves Extract as a Commendable and Green Inhibitor for X70 Steel Corrosion in Hydrochloric Acid. *J. Mol. Liq.* **2021**, *321*, 114914.
(66) Barsoukov, E.; Macdonald, J. R. *Impedance Spectroscopy: theory, Experiment, and Applications*, John Wiley & Sons, 2018.
(67) Cesiulis, H.; Tsyntsaru, N.; Ramanavicius, A.; Ragoisha, G.The Study of Thin Films by Electrochemical Impedance Spectroscopy-*Nanostructures and Thin Films for Multifunctional Applications. NanoScience and Technology*Tiginyanu, I.; Topala, P.; Ursaki, V.Eds.SpringerCham2016342
(68) Al-Amiery, A.; Salman, T. A.; Alazawi, K. F.; Shaker, L. M.; Kadhum, A. A. H.; Takriff, M. S. Quantum Chemical Elucidation on Corrosion Inhibition Efficiency of Schiff Base: DFT Investigations Supported by Weight Loss and SEM Techniques. *Int. J. Low-Carbon Technol.* **2020**, *15* (2), 202−209.
(69) Al-Amiery, A. A.; Shaker, L. M.; Kadhum, A. H.; Takriff, M. S. Exploration of Furan Derivative for Application as Corrosion Inhibitor for Mild Steel in Hydrochloric Acid Solution: Effect of Immersion Time and Temperature on Efficiency. *Mater. Today Proc.* **2021**, *42*, 2968−2973.
(70) Kahlouche, A.; Ferkous, H.; Delimi, A.; Djellali, S.; Yadav, K. K.; Fallatah, A. M.; Jeon, B.-H.; Ferial, K.; Boulechfar, C.; Ben Amor, Y.; Benguerba, Y. Molecular Insights through the Experimental and Theoretical Study of the Anticorrosion Power of a New Eco-Friendly Cytisus Multiflorus Flowers Extract in a 1 M Sulfuric Acid. *J. Mol. Liq.* **2022**, *347*, 118397.
(71) Elaryian, H. M.; Bedair, M. A.; Bedair, A. H.; Aboushahba, R. M.; Fouda, A. E.-A. S. Synthesis, Characterization of Novel Coumarin Dyes as Corrosion Inhibitors for Mild Steel in Acidic Environment: Experimental, Theoretical, and Biological Studies. *J. Mol. Liq.* **2022**, *346*, 118310.
(72) Khodyrev, Y. P.; Batyeva, E. S.; Badeeva, E. K.; Platova, E. V.; Tiwari, L.; Sinyashin, O. G. The Inhibition Action of Ammonium Salts of O, O′-Dialkyldithiophosphoric Acid on Carbon Dioxide Corrosion of Mild Steel. *Corros. Sci.* **2011**, *53* (3), 976−983.
(73) Jebali, Z.; Ferkous, H.; Zerroug, M.; Boublia, A.; Delimi, A.; Bouzid, A.; Majdoub, H.; Ernst, B.; Elboughdiri, N.; Benguerba, Y. Unveiling the Potent Corrosion-Inhibiting Power of Ammophila Arenaria Aqueous Extract for Mild Steel in Acidic Environments: An Integrated Experimental and Computational Study. *J. Environ. Chem. Eng.* **2024**, *12*, 112374.
(74) Elboughdiri, N.; Lakikza, I.; Boublia, A.; Aouni, S. I.; Hammoudi, N. E. H.; Georgin, J.; Franco, D. S. P.; Ferkous, H.; Ghernaout, D.; Benguerba, Y. Application of Statistical Physical, DFT Computation and Molecular Dynamics Simulation for Enhanced Removal of Crystal Violet and Basic Fuchsin Dyes Utilizing Biosorbent Derived from Residual Watermelon Seeds (Citrullus Lanatus). *Process Saf. Environ. Prot.* **2024**, *186*, 995−1010.
(75) Chauhan, D. S.; Mazumder, M. A. J.; Quraishi, M. A.; Ansari, K. R. Chitosan-Cinnamaldehyde Schiff Base: A Bioinspired Macromolecule as Corrosion Inhibitor for Oil and Gas Industry. *Int. J. Biol. Macromol.* **2020**, *158*, 127−138.
(76) Kokalj, A.; Lozinšek, M.; Kapun, B.; Taheri, P.; Neupane, S.; Losada-Pérez, P.; Xie, C.; Stavber, S.; Crespo, D.; Renner, F. U.; Mol, A.; Milošev, I. Simplistic Correlations between Molecular Electronic Properties and Inhibition Efficiencies: Do They Really Exist? *Corros. Sci.* **2021**, *179*, 108856.
(77) Radjai, M.; Ferkous, H.; Zerroug, M.; Djellali, S.; Chaouch, M. A.; Hattabi, B.; Majdoub, H.; Boutahala, M. Methanolic Extract of Artemisia Herba Alba as Eco-Friendly Inhibitor of Carbon Steel Corrosion in 1M HCl Media. In *Recent Advances in Environmental Science from the Euro-Mediterranean and Surrounding Regions: proceedings of Euro-Mediterranean Conference for Environmental Integration (EMCEI-1), Tunisia 2017*; Springer, 2018; pp. 13791381.
(78) Lemaoui, T.; Boublia, A.; Lemaoui, S.; Darwish, A. S.; Ernst, B.; Alam, M.; Benguerba, Y.; Banat, F.; AlNashef, I. M. Predicting the CO2 Capture Capability of Deep Eutectic Solvents and Screening over 1000 of Their Combinations Using Machine Learning. *ACS Sustainable Chem. Eng.* **2023**, *11*, 9564−9580.
(79) Lemaoui, T.; Darwish, A. S.; Almustafa, G.; Boublia, A.; Sarika, P. R.; Jabbar, N. A.; Ibrahim, T.; Nancarrow, P.; Yadav, K. K.; Fallatah, A. M.; Abbas, M.; Algethami, J. S.; Benguerba, Y.; Jeon, B. H.; Banat, F.; AlNashef, I. M. Machine Learning Approach to Map the Thermal Conductivity of over 2,000 Neoteric Solvents for Green Energy Storage Applications. *Energy Storage Mater.* **2023**, *59*, 102795.
(80) Boublia, A.; Lemaoui, T.; Abu Hatab, F.; Darwish, A. S.; Banat, F.; Benguerba, Y.; AlNashef, I. M. Molecular-Based Artificial Neural Network for Predicting the Electrical Conductivity of Deep Eutectic Solvents. *J. Mol. Liq.* **2022**, *366*, 120225.
(81) Lemaoui, T.; Boublia, A.; Darwish, A. S.; Alam, M.; Park, S.; Jeon, B.-H.; Banat, F.; Benguerba, Y.; AlNashef, I. M. Predicting the Surface Tension of Deep Eutectic Solvents Using Artificial Neural Networks. *ACS Omega* **2022**, *7*, 32194−32207.
(82) Costa, J. M.; Lluch, J. M. The Use of Quantum Mechanics Calculations for the Study of Corrosion Inhibitors. *Corros. Sci.* **1984**, *24* (11), 929−933.
(83) Kumar, D.; K, V. M.; Jain, V.; Rai, B. Integrating Experiments, DFT and Characterization for Comprehensive Corrosion Inhibition Studies − A Case for Cinnamaldehyde as an Excellent Green Inhibitor for Steels in Acidic Media. *Corros. Sci.* **2022**, *208*, 110623.
(84) Kokalj, A. On the Alleged Importance of the Molecular Electron-Donating Ability and the HOMO−LUMO Gap in Corrosion Inhibition Studies. *Corros. Sci.* **2021**, *180*, 109016.
(85) Boublia, A.; Guezzout, Z.; Haddaoui, N.; Badawi, M.; Darwish, A. S.; Lemaoui, T.; Banat, F.; Yadav, K. K.; Jeon, B.-H.; lboughdiri, N.; et al. Enhancing Precision in PANI/Gr Nanocomposite Design: Robust Machine Learning Models, Outlier Resilience, and Molecular Input Insights for Superior Electrical Conductivity and Gas Sensing Performance. *J. Mater. Chem. A* **2024**, *12*, 2209−2236.
(86) Yasmin, T.; Mahmood, A.; Farooq, M.; Rehman, U.; Sarfraz, R. M.; Ijaz, H.; Akram, M. R.; Boublia, A.; Bekhit, M. M. S.; Ernst, B.; et al. Quince Seed Mucilage/β-Cyclodextrin/Mmt-Na+-Co-Poly (Methacrylate) Based PH-Sensitive Polymeric Carriers for Controlled Delivery of Capecitabine. *Int. J. Biol. Macromol.* **2023**, *253*, 127032.
(87) Obot, I. B.; Macdonald, D. D.; Gasem, Z. M. Density Functional Theory (DFT) as a Powerful Tool for Designing New Organic Corrosion Inhibitors. Part 1: An Overview. *Corros. Sci.* **2015**, *99*, 1−30.
(88) Mamand, D. M.; Qadr, H. M. Corrosion Inhibition Efficiency and Quantum Chemical Studies of Some Organic Compounds: Theoretical Evaluation. *Corros. Rev.* **2023**, *41*, 427−441.
(89) Mouffok, A.; Bellouche, D.; Debbous, I.; Anane, A.; Khoualdia, Y.; Boublia, A.; Darwish, A. S.; Lemaoui, T.; Benguerba, Y. Synergy of Garlic Extract and Deep Eutectic Solvents as Promising Natural Antibiotics: Experimental and COSMO-RS. *J. Mol. Liq.* **2023**, *375*, 121321.

https://doi.org/10.1021/acsomega.3c10240
ACS Omega 2024, 9, 27945−27962

(90) Uka, D.; Blagojević, B.; Alioui, O.; Boublia, A.; Elboughdiri, N.; Benguerba, Y.; Jurić, T.; Popović, B. M. An Innovative and Environmentally Friendly Approach for Resveratrol Solubilization and Bioaccessibility Enhancement by Using Natural Deep Eutectic Solvents. *J. Mol. Liq.* **2023**, *391*, 123411.
(91) Yang, W.; Cohen, A. J.; De Proft, F.; Geerlings, P. Analytical Evaluation of Fukui Functions and Real-Space Linear Response Function. *J. Chem. Phys.* **2012**, *136*, 144110.
(92) Zhang, Q. H.; Hou, B. S.; Li, Y. Y.; Lei, Y.; Wang, X.; Liu, H. F.; Zhang, G. A. Two Amino Acid Derivatives as High Efficient Green Inhibitors for the Corrosion of Carbon Steel in CO2-Saturated Formation Water. *Corros. Sci.* **2021**, *189*, 109596.
(93) Murmu, M.; Murmu, N. C.; Ghosh, M.; Banerjee, P. Density Functional Theory, Monte Carlo Simulation and Non-Covalent Interaction Study for Exploring the Adsorption and Corrosion Inhibiting Property of Double Azomethine Functionalised Organic Molecules. *J. Adhes. Sci. Technol.* **2022**, *36* (23−24), 2732−2760.
(94) Ferkous, H.; Sedik, A.; Delimi, A.; Redjemia, R.; Abdesalem, K.; Boulechfar, C.; Abdennouri, A.; Madaci, A.; Berredjem, M.; Boublia, A.; et al. A Comparative Study of Novel Synthesized Sulfamide Compounds: Electrochemical, Morphological, XPS, and Theoretical Investigations on Copper Corrosion Inhibition in 1.0 M HCl. *J. Mol. Liq.* **2024**, *394*, 123781.
(95) ¸ahin, E. A.; Solmaz, R.; Gecibesler, I. H.; Kardą, G. Adsorption Ability, Stability and Corrosion Inhibition Mechanism of Phoenix Dactylifera Extrat on Mild Steel. *Mater. Res. Express* **2020**, *7* (1), 16585.
(96) Dotto, G. L.; Pinto, L. A. A.; Hachicha, M. A.; Knani, S. New Physicochemical Interpretations for the Adsorption of Food Dyes on Chitosan Films Using Statistical Physics Treatment. *Food Chem.* **2015**, *171*, 1−7.
(97) Pang, X.; Sellaoui, L.; Franco, D.; Netto, M. S.; Georgin, J.; Luiz Dotto, G.; Abu Shayeb, M. K.; Belmabrouk, H.; Bonilla-Petriciolet, A.; Li, Z. Preparation and Characterization of a Novel Mountain Soursop Seeds Powder Adsorbent and Its Application for the Removal of Crystal Violet and Methylene Blue from Aqueous Solutions. *Chem. Eng. J.* **2020**, *391*, 123617.
(98) dos Reis, G. S.; Grigore Cazacliu, B.; Rodriguez Correa, C.; Ovsyannikova, E.; Kruse, A.; Lima, E. C.; Dotto, G. L. Adsorption and Recovery of Phosphate from Aqueous Solution by the Construction and Demolition Wastes Sludge and Its Potential Use as Phosphate-Based Fertiliser. *J. Environ. Chem. Eng.* **2020**, *8* (1), 103605.
(99) Tran, H. N.; Nguyen, H. C.; Woo, S. H.; Nguyen, T. V.; Vigneswaran, S.; Hosseini-Bandegharaei, A.; Rinklebe, J.; Kumar Sarmah, A.; Ivanets, A.; Dotto, G. L.; et al. Removal of Various Contaminants from Water by Renewable Lignocellulose-Derived Biosorbents: A Comprehensive and Critical Review. *Crit. Rev. Environ. Sci. Technol.* **2019**, *49* (23), 2155−2219.

https://doi.org/10.1021/acsomega.3c10240
ACS Omega 2024, 9, 27945−27962